Daniel Gütl BSc

# Investigation of Nicotinic Receptors in the Locusts optic lobe by Immunohistochemistry

**MASTERARBEIT**

Zur Erlangung des akademischen Grades

Master of Science

Masterstudium Biochemie und Molekulare Biomedizin

eingereicht an der

**Technischen Universität Graz**

Betreuer

Ass.Prof. Priv.-Doz. Mag. Dr.rer.nat. Gerd Leitinger

Graz, April 2016

## EIDESSTATTLICHE ERKLÄRUNG

Ich erkläre an Eides statt, dass ich die vorliegende Arbeit selbstständig verfasst, andere als die angegebenen Quellen/Hilfsmittel nicht benutzt, und die den benutzten Quellen wörtliche und inhaltlich entnommene Stellen als solche kenntlich gemacht habe. Das in TUGRAZonline hochgeladene Textdokument ist mit der vorliegenden Masterarbeit identisch.

Datum

Unterschrift

# Danksagung

Während der Zeit der Masterarbeit am Institut für Histologie, Zellbiologie und Embryologie an der Medizinischen Universität Graz habe ich viele hilfsbereite Menschen kennengelernt die mich offen und freundlich in Ihren Kreis aufgenommen haben. Ein großes Danke an dieser Stelle all jenen die ich hier nicht namentlich erwähnen kann.

Meinen Eltern gebührt besonderer Dank, da sie mich immer in allem unterstützt haben und mir den Rückhalt gegeben haben den es brauchte um meine Ziele zu verwirklichen. Ohne sie wäre meine Ausbildung nicht möglich gewesen.

Besonderer Dank gebührt meinem Betreuer Gerd Leitinger für dieses interessante Thema und die Möglichkeit mich selbst mit Ideen einzubringen. Er war bei Problemen immer eine wichtige Stütze und konnte mir oft weiterhelfen.

Bei der Durchführung aller Laborarbeiten war das ELMI-Team immer für mich da, Danke Elisabeth Bock, Elisabeth Pritz und Dominique Pernitsch. Die bei euch gelernten Arbeitstechniken werden mich auf meinem weiteren Weg in der Elektronenmikroskopie immer begleiten.

Bedanken möchte ich mich auch bei Stefan Wernitznig und allen anderen Masterstudenten und auch Bachelorstudenten mit denen ich viel Zeit während der Arbeit verbracht habe. Die Mittagspausen wären nicht diesselben gewesen ohne euch.

Weiters möchte ich noch Walter Kaufmann vom IST Austria danken für den Support bei der Silber-Amplifizierung, ohne sein Fachwissen hätte sich dieser entscheidende Schritt weitaus komplizierter dargestellt.

Zuletzt ein großes Danke an alle meine Freunde, schön dass ihr immer ein offenes Ohr habt und Freizeit für gemeinsame Abenteuer am Fels.

## Abstract

The natural circuitry in the optic lobe of the desert locust, *Schistocerca gregaria*, is of great interest as this animal is a model organism for collision avoidance in a biological system. Collision detection in animals is useful to avert danger and warn the animal of nearing predators. It is a system that evolved over time and works reliably in many different situations. The collision detecting neuronal circuit of locusts is simple enough to aim for a good understanding of its different parts, yet some of the neurons are big enough to be easily accessible for sample preparation and experiments.

To understand how such a system works, we have to look at the path of the signal, from the light that enters the eye to the cells controlling the motoneurons of legs and wings.

In the locust there are three optical neuropils, the lamina, medulla and lobula complex all connected via neurons. For collision detection, trans-medullary afferent neurons (TMAs) conduct signals about changes in light intensity from other neurons underneath the insect's eye to the lobula giant movement detector neurons (LGMD 1 and 2). The LGMD 1 is a neuron that receives input from thousands of TMAs and conducts the signal on a one to one basis to the descending contralateral movement detector (DCMD) neuron which is then connected to motoneurons. The synaptic connection between TMAs and the LGMDs use acetylcholine (ACh) as neurotransmitter.

It must be possible for the whole system to differentiate between a collision and a false alarm, such as an object that is passing by. It was proposed that this is achieved by TMAs which can excite the LGMDs and at the same time inhibit each other. This process called lateral inhibition and its detailed mechanisms is not fully understood. In this system, the insect nicotinic acetylcholine receptor (nAChR) is essential in the process of signal transduction at the synapse level, at the cell membrane of the LGMDs and perhaps also of the afferent neurons. The work of this thesis concentrates on the location of the nicotinic receptors in the synapses between the trans-medullary afferent cells and the LGMD to gain a better understanding of the current model.

I prepared sections of the brain, embedded them in gelatin and labeled them with two markers specific to the Bruchpilot protein and nicotinic acetylcholine receptors. I demonstrated with Confocal Laser Scanning Microscopy (CLSM) that the antibodies bind specifically to the target areas and labelled the markers with gold probes to examine them with the electron microscope.

The resulting thesis contains detailed working protocols that could be used to investigate this system further in the future. It would be possible to look for the muscarinic receptors in the synapse or to do a study with higher resolution electron tomography.

## Zusammenfassung

Ein natürlicher Schaltkreis aus Nervenzellen im optischen Lappen der Wüstenheuschrecke (*Schistocerca gregaria*) dient als Modell für Kollisionserkennung. Kollisionsdetektion und -vermeidung in Insekten ist notwendig, um Gefahren für das Tier, wie herannahende Fressfeinde zu erkennen. Das zugrundeliegende System aus Neuronen hat sich über die Zeit entwickelt und funktioniert zuverlässig in vielen unterschiedlichen Situationen. Dieses spezielle Netzwerk in der Heuschecke ist einfach genug, um seine Bestandteile identifizieren zu können, und manche seiner Neurone sind groß genug, um sie zugänglich zu machen für gezielte Probenvorbereitung wo es darauf ankommt, einzelne Zellen oder Bereiche des optischen Lappens zu identifizieren.

Um zu verstehen, wie dieses System funktioniert, müssen wir herausfinden, wie die Information, die von den Augen aufgenommen werden, über das Netzwerk aus Zellen zu den Motorneuronen der Beine und Flügel der Heuschrecke transportiert und währenddessen prozessiert wird.

In der Heuschecke gibt es drei optische Neuropile, die Lamina, Medulla und den Lobula Komplex welche über Neurone verbunden sind. Derzeitiger Stand ist, dass trans-medulläre afferente Zellen (TMAs), Signale von unter dem Insektenauge gelegenen Nervenzellen zu den sogenannten lobula giant movement detector Nervenzellen (LGMD 1 und 2) weiterleiten. Das LGMD 1 bekommt Signale von tausenden dieser TMAs und leitet dann ein Signal an das descending contralateral movement detector Neuron (DCMD) weiter, welches mit den Motorneuronen verknüpft ist. Die Verbindung zwischen TMAs und LGMDs wird durch Synapsen geknüpft welche Acetylcholin (ACh) als Neurotransmitter verwenden.

Die Verknüpfung aller an diesem System beteiligter Nervenzelle muss es möglich machen, dass zwischen einer drohenden und einer beinahe Kollision unterschieden werden kann. Dies wird nach einer gängige Hypothese dadurch erreicht, dass TMAs das LGMD erregen können, aber gleichzeitig benachbarte TMAs inhibieren können. Dieser Prozess der lateralen Inhibition und der zugrundeliegende Mechanismus sind noch nicht vollkommen verstanden. Ein wichtiger Bestandteil der Synapse und somit der Signalweiterleitung ist der nikotinische Acetylcholin Rezeptor (nAChR). Dieses Transmembranprotein spielt eine wichtige Rolle in den Zellmembranen der LGMDs und vielleicht auch TMAs. In der vorliegenden Arbeit habe

ich mich darauf konzentriert, diese Proteine in den Nervenzellen der Heuschrecke zu lokalisieren.

Es wurden Schnitte des Hirns der Heuschrecke angefertigt, diese in Gelatine ausgegossen und anschließend mit zwei verschiedenen Markern, einer spezifisch für das Bruchpilot Protein, der andere für nikotinische Acetylcholin Rezeptoren, markiert. Mit dem Konfokalen Laser Scanning Mikroskop (CLSM) wurde gezeigt, dass diese Antikörper spezifisch binden. Um mehr Auflösung zu bekommen wurde dann in die Elektronenmikroskopie gewechselt und mit Gold Nanopartikeln diesselben Proteine markiert und detektiert.

Die vorliegende Arbeit beschreibt im Detail alle nötigen Protokolle, um dieses System in Zukunft mit CLSM und Elektronenmikroskopie weiter zu untersuchen. Es wäre möglich, diese Protokolle auf andere wichtige Proteine, wie zum Beispiel den muskarinischen Acetylcholin Rezeptor auszuweiten und noch höher aufgelöste Elektronentomographie durchzufühen.

# Table of contents

# 1. Introduction

In nature the need to advance biological systems is ever present. During evolution, predators improve their speed and prey improve mechanisms of evasion. These mechanisms are not always trained or learned during animal life, but have roots in the anatomy and biochemistry of their cells. Motion detection in the visual system is one of the most important sensory systems for predator avoidance, at it is often used to avert danger.

Understanding how information is processed in the brain of an animal is a goal that can be studied on several levels: behavioural, physiological and anatomical studies have all contributed to the view we have at the moment. In the recent past computations with neuronal circuits tried to emulate these natural mechanisms by which animals avoid predators, but they need detailed information how the signals travel within the neural systems and how their cells are connected. Even after a half century of investigations the motion detection system of insects are not well understood and there remains much work to be done (Takemura et al., 2013).

To understand how this works, one has to elucidate how sensory input is filtered and how the system tells the animal what reaction to the optical input is the best course of action. Not every signal has to elicit a reaction and in some cases the reaction is not one that saves the animal from harm as predators also can adapt. This shows that these systems have limits but are designed to work reliably in a lot of different situations.

## 1.1 Schistocerca Gregaria as a Model Organism

In this study the movement detection system of the desert locust (*Schistocerca gregaria*) is of interest. It consists of a neuronal circuit situated in different parts in the brain that are easy to dissect and identify (Fig. 1). Locusts travel in large swarms where they need to detect objects approaching on a collision course to avoid dangers. At the same time they do not need to react to movement of other locusts around them as long as the other locusts do not cross their path (Judge and Rind, 1997). The collision detector in the optical pathway of the locust was described before (O'Shea and Williams, 1974; Rind and Simmons, 1992; Rowell, 1971) and has since been the target of a lot of further investigations (Chan and Gabbiani, 2013; Rind and Simmons, 1999).

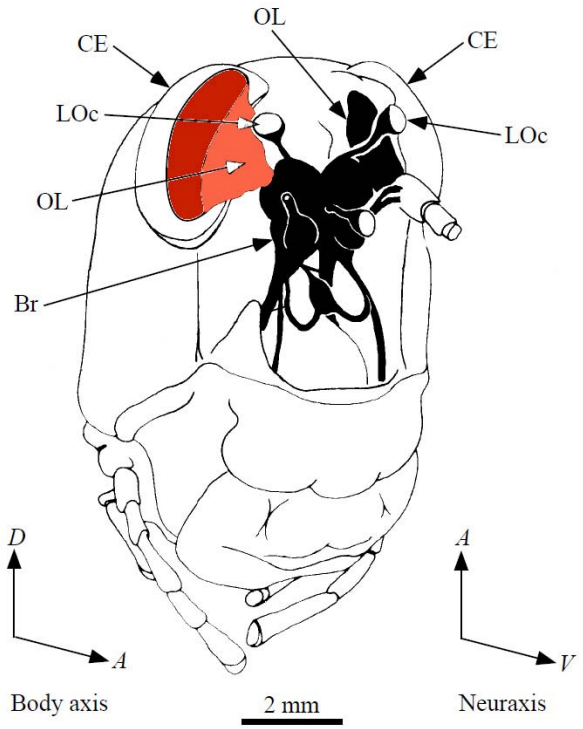


**Figure 1: Diagram of the locust brain and its orientation in the head in respect to body axis and neuraxis. Optic lobe (OL) is colored in red. The OL is positioned between the compound Eyes (CE) and Brain (Br). Modified after (Elphick et al., 1996).**

There are many ways to investigate this system, for instance with immunohistochemistry (Rind and Leitinger, 2000) neurotransmitters or their receptors can be localized. The methods of choice here are light and electron microscopy.

Electrophysiology (Rind, 1984) can be used to see the change of electric potential in a cell after a certain event has happened, for instance the compound eye of the locust sees a dark object that is rapidly growing in size in its field of view (an approach). This will result in spikes in the cells of the movement detection pathway and give clues to what is happening when signals are transmitted between the neurons of the pathway. Another technique is the patch-clamp, where neurons are dissected and then a microelectrode attached to the cell membrane. With this the currents generated by a single transmembrane protein, for example an ion-channel receptor, can be measured. The cell can then be perfused with different chemicals to test whether these are agonists or antagonists of the protein (Benson, 1992; Coggan et al., 1997; Thany et al., 2007).

Serial block face scanning electron microscopy (SBEM) (Denk and Horstmann, 2004; Wernitznig et al., 2015) is best when it comes to elucidating the connection of several cells. A whole volume of tissue can be imaged in slices and then single cells and their synaptic connections reconstructed using a computer. With this anatomy of the cells and their synaptic connections are easy to visualize in 3D and statistics can show how many synapses are in certain volume of the tissue.

## 1.2 Collision detection in the locust

It is known that locusts can sense impending collision (Rind and Bramwell, 1996) and that this mechanism is present in the different instar stages of the developing animal (Sztarker and Rind, 2014). The calculation if a collision is imminent happens in trans-medullary afferent cells and a pair of special neurons, the Lobula Giant Movement Detector 1 and 2 (LGMD 1 and 2). If an object is on a collision course then the sum of signals generated by the thousands of afferent cells rises and excites the LGMD 1 more and more leading to a train of action potentials with increasing frequency. If the approach is a near miss the sum of the

input from afferent neurons in the LGMD 1 will not rise to the point where as many action potentials are generated. The action potentials of the LGMD 1 are then transferred to the Descending contralateral Movement Detector (DCMD), a neuron postsynaptic to the LGMD 1, on a one to one basis (Rind, 1984).

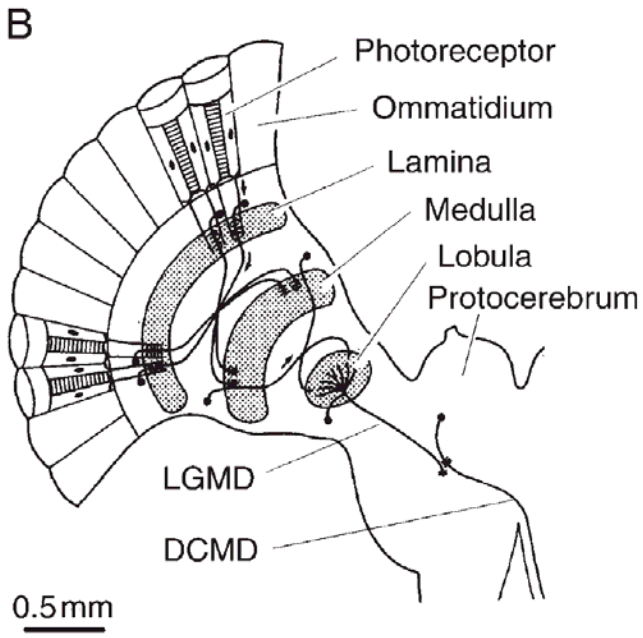


**Figure 2: Schematic illustration of the locust visual system viewed from behind. From (Rind and Simmons, 1999)**

The compound eye of the locust (Fig. 2) consists of approximately 8500 single facets, each one about 1.25° separated from its neighbors optical path (Wilson et al., 1978). Beneath the eyes there are eight light gathering photoreceptors and they all contribute to a single rhabdome. Six photoreceptors are connected to the first neuropil, the lamina. The other two go through the lamina into the medulla, the second optic neuropil (Wilson et al., 1978). In the medulla it is believed that the first motion computation takes place, done by small-field neurons (James and Osorio, 1996; Osorio, 1986). The problem with these cells is that they are too small for electrophysiological experiments, so it is easier to record electrophysiologically from the LGMD 1 and 2 cells in the lobula complex, which is the third optic neuropil (O'Shea and Williams, 1974). Both cells represent parallel signal processing and have no known interconnection or synapses with one another (Rind, 1987). They share

the same excitatory input organization and thus elicit similar responses to signals from the eyes (Rind and Simmons, 1997).

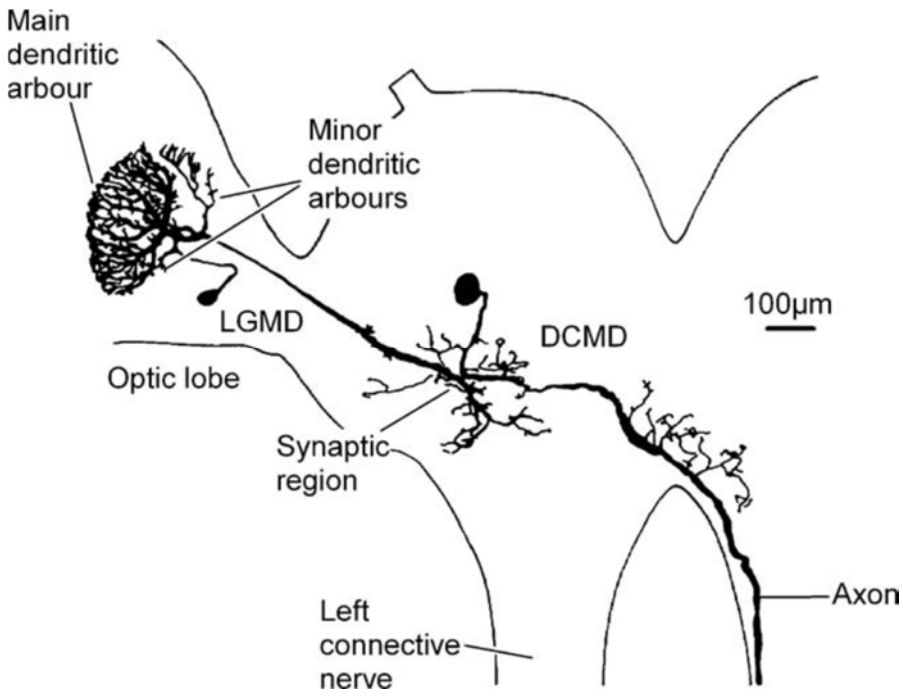


**Figure 3: LGMD and DCMD, the signal travels along these cells to the Axon leading to the motor neurons. from (Rind, 1984)**

After the LGMD 1 the DCMD neuron is excited (Fig. 3). The synapse between these two cells consists of upwards to 2250 contacts (Killmann et al., 1999). The DCMD then projects then into the thoracic ganglia and has output connections to motoneurons and interneurons controlling leg and flight behavior (Burrows and Rowell, 1973; Rind and Simmons, 1999).

## 1.3 Acetylcholine Receptors

The nicotinic acetylcholine receptor (nAChR) is a member of the cys-loop superfamily of ligand-gated ion channels. It consists of an assembly of five transmembrane subunits that form a channel across the cell membrane. In a passive or resting state this channel is closed. Activation happens by neurotransmitter molecules, most notably acetylcholine (ACh) or nicotine, this results in a conformational change and in opening of the central channel. This channel transports cations ($Ca^{2+}$ and $Na^{+}$) into the cell (Jones et al., 2002).
It is known that ACh activates both nicotinic and muscarinic receptors, both in the insect and the mammalian central nervous system (CNS). They can be either presynaptic or postsynaptic (Clarke and Pert, 1985) and have different roles depending on their location. The muscarinic acetylcholine receptors (mAChRs) are G-protein coupled receptor that perform different roles specified by their location in the membrane (Trimmer, 1995).

At the postsynaptic level nAChR are associated with mediated excitation and membrane depolarization while mAChR are associated with hyperpolarization. Presynaptic, the activation of nAChRs could produce either excitation or inhibition through the release of other neurotransmitters. Properly timed nAChR activity ($Ca^{2+}$ influx) could ensure that the right amount of neurotransmitter is released and thus increases the chance that important events (like an action potential) at a synapse take place (Wonnacott, 1997).

In a traditional synapse the ACh released has a very high concentration (up to 100 mM) and the pulse into the confined space of the synaptic cleft is on a millisecond timescale. The ACh will then diffuse 10-20 nm in less than 0.2 ms and target the postsynaptic receptors. (Vizi and Lendvai, 1999).

The possibility that presynaptic nAChRs exist in insects is still debated, but it is assumed that the postsynaptic neurons have receptors with a nicotinic pharmacology that are mediating excitatory postsynaptic potentials (EPSPs) (Trimmer, 1995) and that the receptors at the presynaptic site often have a muscarinic profile. These receptors have the same profile as the mammalian M2-subtype as was proven in *Locusta migratoria* (Knipper and Breer, 1989),

so for further investigation one should concentrate on homologous insect receptors of this type.

For labelling nAChRs, α - Bungarotoxin (α-BTX) is a neurotoxin that has been shown to label nAChRs in the rat using fluorescence and electron microscopy (Jones and Wonnacott, 2004). Labelling only works if the receptors contain the alpha7-subunit, to which α -BTX is specific for (Coggan et al., 1997). In *Locusta migratoria* it was shown (Benson, 1992) that α -BTX also is a strong antagonist of nAChR and so it was a prime candidate to visualize the receptors. For *Schistocerca gregaria*, the *Sg*α1 receptor subunit was identified and cloned into *Xenopus* oocytes. It was shown that it could be completely blocked by α -BTX (Marshall et al., 1990).

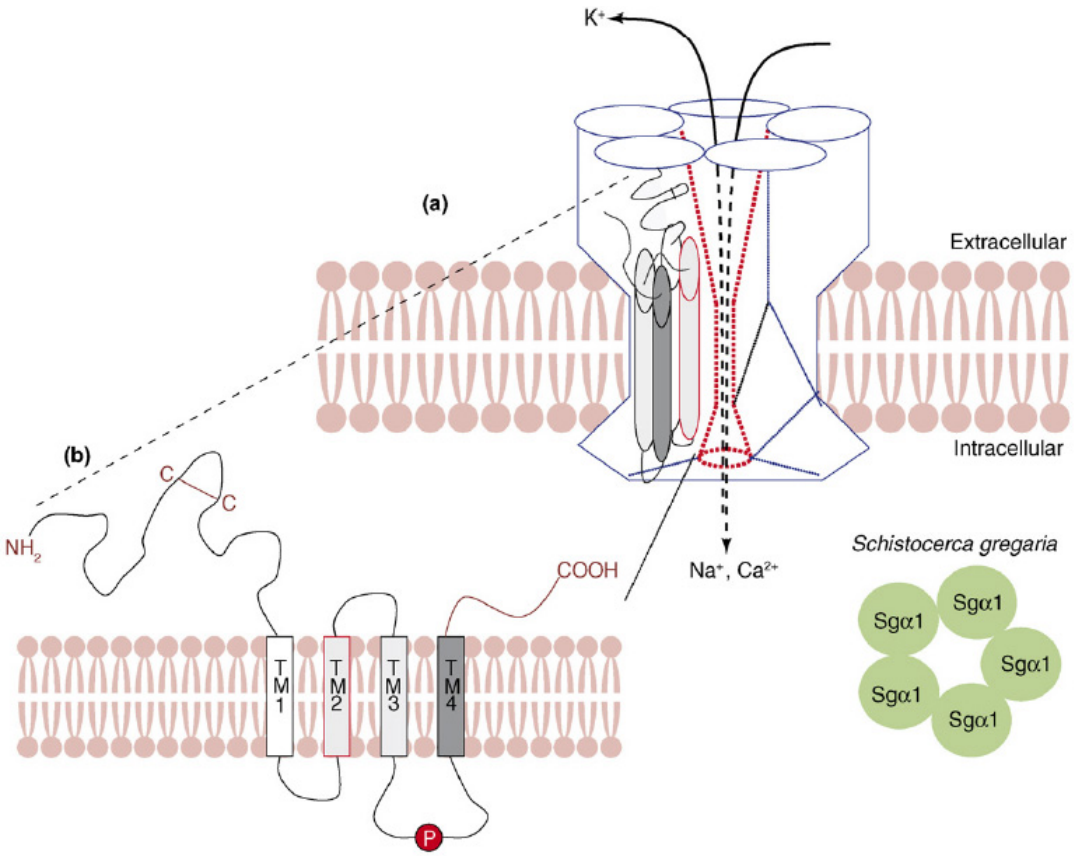


**Figure 4: a) the nACh receptors have 5 subunits, in the case of *Schistocerca gregaria* the α -BTX sensitive receptor consists of identical subunits arranged around the central ion channel, which is selective for $Na^+$, $K^+$ and $Ca^{2+}$. b) Each of this subunits has 4 separate transmembrane domains. The binding site for α -BTX is thought to be between two of those subunits. It is believed that homomeric receptors all are α -BTX sensitive if the subunits they are composed of are homologous to the α7. from (Thany et al., 2007)**

## 1.4 Lateral Inhibition

The most critical image cues for a response of the LGMD/DCMD are fast moving edges and rapidly increasing image edges, whose size increases at an ever increasing speed, as is the case for an object on a collision course (Rind and Simmons, 1992).

(Rind and Bramwell, 1996) concluded that lateral inhibition between afferent cells is needed to distinguish between an object approaching and an object passing by. According to the model of the LGMD devised in (Rind and Bramwell, 1996), as an edge moves over the eye at a constant speed, there is a race between excitation and inhibition and if there is no speed increase in excitation (as the object passes by and thus its edges don't grow with increasing speed) the inhibition wins the race and thus the excitation of the afferent neurons is suppressed (Rind and Bramwell, 1996). If an object approaches on a collision course, the excitation wins the race due to the edges growing with increasing speed and this causes increasing excitation in ever more single afferent neurons (Rind and Bramwell, 1996). The LGMD sums up the afferent neurons' signals and therefore also becomes excited (Rind and Bramwell, 1996). However, another model mimics many features of the LGMD's excitation pattern without including lateral inhibition (Jones and Gabbiani, 2010).

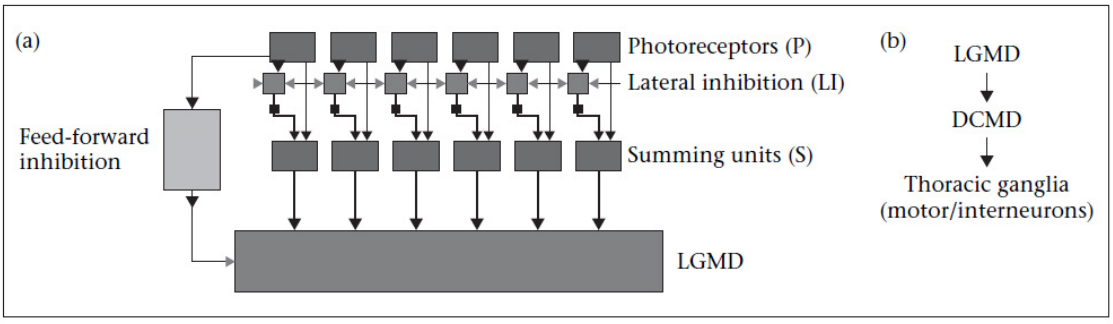


Figure 5: Generalized model of the connectivity in the locust and model LGMDs (Stafford et al., 2007).

There are also feed-forward inhibitory loops between the trans medullary afferent cells (TMA) and the LGMDs (Fig. 5). It is necessary to prevent large excitatory responses of the LGMDs caused by movement of the whole visual field (Rowell et al., 1977). These loops are activated when a large number of receptor units are excited at the same time and they truncate the LGMD's response after an approach has ceased. If one would eliminate the

feed-forward inhibition then the response of the LGMD to receding or approaching objects would be prolonged (Rind and Bramwell, 1996).

In the locust the lateral inhibition was proposed to be realized via reciprocal synapses between TMAs, when one synapse releases its neurotransmitter the other cell next to it is inhibited by the ACh (Rind and Simmons, 1998).

## 1.5 The reciprocal synapse

As can be seen in (Fig. 6 and 7), the TMAs giving input to the LGMD often form reciprocal synapses with other neighbouring TMAs.

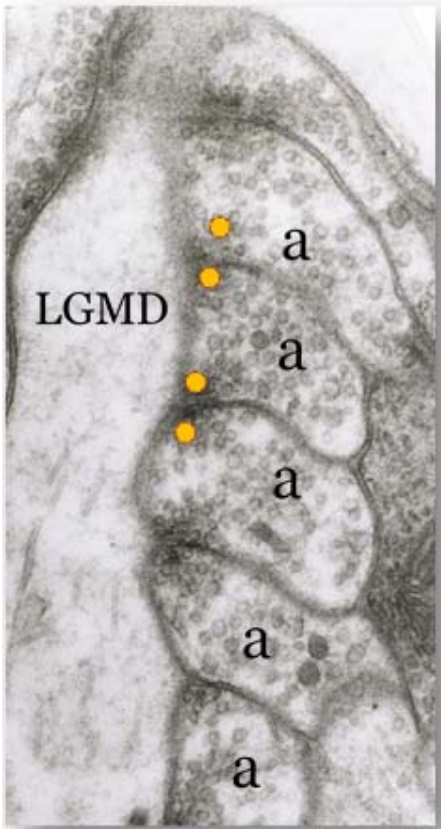


Figure 7: LGMD and TMAs (a) with reciprocal Synapses marked in yellow (Rind and Leitinger, 2000)

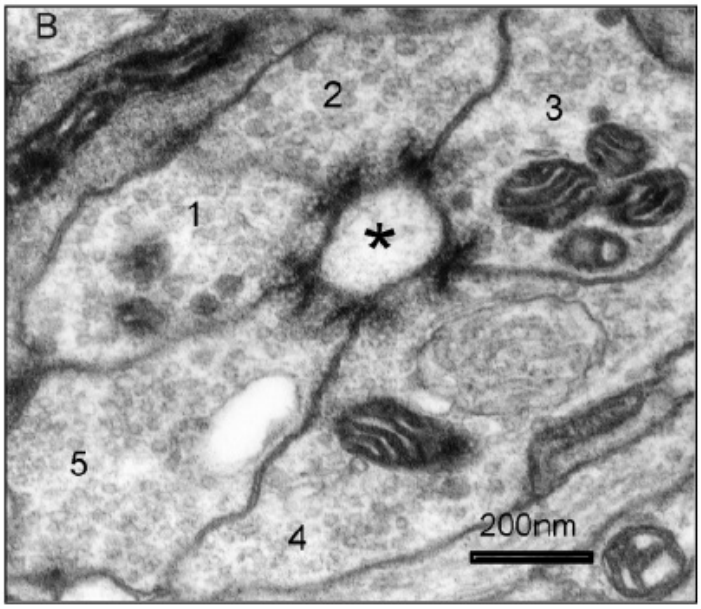


Figure 6: A small LGMD 1 process (asterisk) featuring five reciprocal synapses from 5 TMAs. (Rind, 2002)

The synapses can reach a high densitiy around the many smaller LGMD processes and form cartwheel structures. Intracellular recordings from the LGMD show no excitatory interactions between these TMAs so the current model (Rind and Bramwell, 1996) only

includes inhibition between these cells. If one cell excites the LGMD by activatinig its synapse (releasing ACh) it inhibits the neighbouring cell (Fig. 8), blocking it from releasing its stored neurotransmitter (Rind, 2002; Rind and Simmons, 1998).

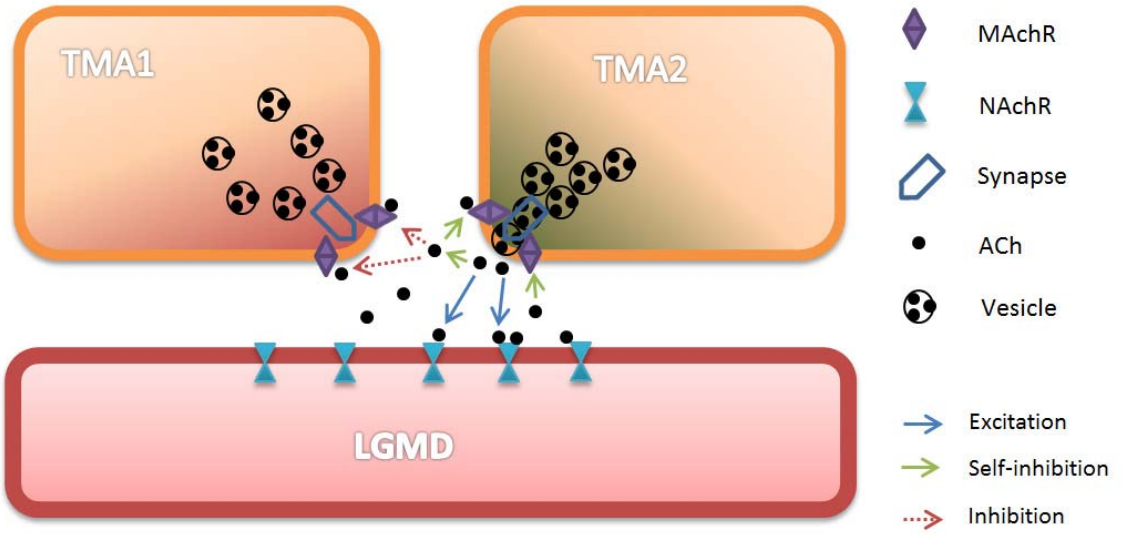


**Figure 8: model of the reciprocal synapse after unpublished results by F. Claire Rind. TMA2 is the active cell releasing its neurotransmitter and TMA1 is the cell that is inhibited by the release of the ACh.**

The action of self-inhibition was first calculated into a model by F. Claire Rind 2016 (unpublished results). The neurotransmitter particles released into the synaptic cleft first reaches the mAChRs in TMA2 (the “active” cell). As the muscarinic receptor is a G-protein coupled receptor there is a time delay so self-inhibition acts fast but doesn’t stop the activation instantly. There is also inhibition of the neighbouring TMA1, as the MAChRs of this cell register the ACh in the synaptic cleft and cause a membrane hyperpolarization.

## 2. Materials and Methods

All experiments were performed with the desert locust (*Schistocerca gregaria*), all the specimen were of the adult population bought from Zoo Muser Graz.

### 2.1 Dissection of *Schistocerca gregaria*

Animals were put on ice for about one minute then decapitated. Afterwards the relevant part of the brain (*Lobus opticus*) was dissected according to the protocol in the appendix. Ice cold insect saline solution (Table 1) was used during each dissection step. Afterwards the parts were placed in 2% formaldehyde (PFA) in 0.1M Phosphate buffer (PB).

**Table 1: ingredients for insect saline solution (100 mL)**

| | [g] |
|---|---|
| NaCl | 1,02 |
| KCl | 0,072 |
| $CaCl_2$ | 0,022 |
| $MgCl_2x6H_2O$ | 0,086 |
| $NaHCO_3$ | 0,007 |
| $Na_2HPO_4x2H_2O_2$ | 0,03 |
| $C_6H_{12}O_6xH_2O$ | 0,77 |

### 2.2 Fluorescence Imaging

To visualize if α-BTX has binding sites close to the LGMD's dendrites in the lobula complex, fluorescence labelling and Confocal Laser Scanning Microscopy was used. This has the advantage that the sample preparation can be done in only 3 days and it gives a good overview of the whole optic lobe. Double labelling experiments with both α-BTX and NC82, a marker for the bruchpilot protein, were also performed.

Following dissection the optic lobe was placed for 3 hours in 2% FA in 0.1 M PB (pH 7.4). No gluraraldehyde (GA) is added due to this chemical causing auto-fluorescence and it is also interacting with the natural binding sites for the bungarotoxin (Jones et al., 2002). Following a one hour rinse with PB the parts are then oriented in liquid 15% gelatin (in PB, heated up

to 40°C) and put on ice for the gelatin to solidify. Orientation in the gelatin can be crucial, depending from what direction one wants to cut the optic lobe.

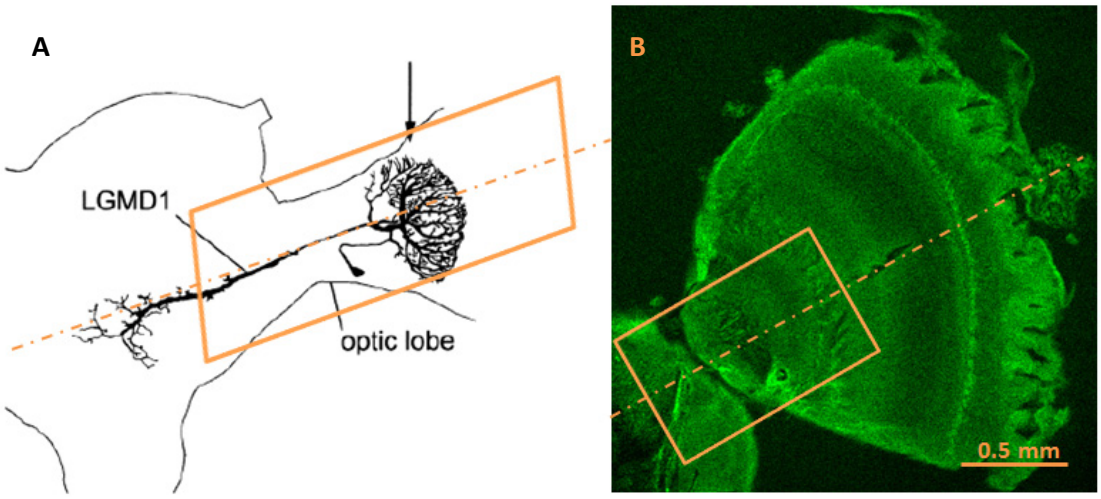


**Figure 9: Left: Location of the LGMD in the optic lobe. Dotted line is the axis of cutting with the vibratome. Modified after Rind and Leitinger, 2000. Right: CLSM Image of a frontal section of the optic lobe (parallel to the drawaing shown in A), Alexa Fluor 488 coupled to α-BTX.**

It might seem easier at first to cut cross sections of the optic lobe, in the direction indicated by the black arrow pointing to the LGMD in (Fig. 9Ai), but as the LGMD is not flat but curved, cutting in the direction of the pointed line in (Fig. 9Ai) resulted in many slices that showed some parts of the LGMD in the microscope later. Interpretation of these sections is also straightforward, as one can distinguish the lamina, medulla and lobula complex easily.

The blocks are then cut with a vibratome in 50-70 µm thick sections. Not every section contains part of the lobula complex, so careful selection under a stereo microscope is needed.

**Table 2: ingredients for Solution1 [100mL] in PBS**

| **Solution1** | |
|---|---|
| Triton X-100 | 100µL |
| BSA | 0.8g |
| Glycine | 0.75g |

The next step is preincubation with 5% normal goat serum in Solution1 (see Table 2) for one hour and afterwards incubation with the first antibody or with α-BTX, diluted in solution1 (Sol1), overnight.

**Table 3: SOP for fluorescence imaging**

| | action/chemicals | temperature | duration |
|---|---|---|---|
| Fixation | 2% PFA, 0.1M PB, pH 7.4 | Room temperature (RT) | 3 h |
| rinse | Rinse in PB | 4° C | 1 h |
| embedding | Gelatine (15% in PB) | on ice | - |
| fixation | 2% PFA, 0.1M PB, pH 7.4 | 4°C | 2 h |
| rinse | Rinse in PB | 4° C | Overnight (ON) |
| cutting | Cut 50-70µm sections with vibratome | 4°C | - |
| make Sol1 | 0.1% Triton X-100, 0.8% Bovine Serum Albumin (BSA) 0.1M glycine in PBS | Store at 4°C | - |
| preincubation | Put section into Sol1 with 5% Goat Serum | RT | 1 h |
| incubation | Incubate overnight with primary antibody diluted in Sol1 | 4°C | ON |
| rinse | 3x PBS | RT | 3x10min |
| incubation | Incubate with secondary antibody diluted in Sol1 | RT | 2 h |
| rinse | 3x PBS | RT | 3x 10min |
| transfer | Transfer to distilled water | RT | - |
| mounting | Mount on microscope slides using ProLong Gold Antifade | RT | |
| sealing | seal the slides with nail polish | RT | - |

To visualize the α-BTX and bruchpilot proteins direct and indirect immunofluorescence was used on the adult locust (Table 3). The bruchpilot protein is a protein that tethers vesicles to the synapse (Kittel, 2006) and can be detected in the locust by the NC82 antibody (Leitinger et al., 2012), a gift from Prof. Buchner, Würzburg, Germany. It is available in the Hybridoma Bank under the antibody ID AB_2314866. α-BTX has been shown to label the nicotinic ACh receptors (Young et al., 2003).

For direct immunofluorescence we purchased α-BTX covalently linked to Alexa Fluor 488 or Atto633 fluorosphores. Because the NC82 antibody was not linked to a fluorophore, indirect immunofluorescence was needed for labelling with this antibody. Its host species is mouse and thus it could be coupled with Cy3 and Cy2 goat anti-mouse fluorescent dyes in a further incubation step. This second incubation is carried out on the next day after a rinse with PBS (3x10min).

After the last rinse the sections are transferred to distilled water and then carefully mounted on microscope slides, using ProLong Gold Antifade as mounting medium. The sections must cure for 24 hours and can then be sealed with nail polish on the sides of the coverslip.

### 2.2.1 Leica SP2 Confocal Laser Scanning Microscope

All images were taken with the Leica TCS SP2 Microscope, using the Leica Laser Scanning Software. In addition to single images, stacks of multiple images in varying probe depths were recorded so as to show the changes in signal intensity inside the tissue. This so called z-stack scan is a feature of the laser scanning microscope, as only one point of the imaged sample is illuminated at one time at a defined focal plane and so all the points in x-y direction can be imaged in sequence, and afterwards the corresponding x-y points in another focal plane (z-direction) can be imaged. With the Huygens Essential Software it is then possible to render these stacks in 3D.

For double labelled probes (e.g. labelling with α-BTX and NC82 antibody together, with different fluorosphores) the problem of fluorescence crosstalk can occur. Crosstalk occurs when the emission and excitation of two fluorescent dyes are too close. Signal from one dye gets detected in the channel of the other. To circumvent this, the different emission lines were imaged in sequence one after another in between frames.

Even if using an antifade-reagent, fluorescence photo bleaching can occur, especially when illuminating the same field of view multiple times for the production of z-stacks. Laser intensity always needed to be carefully adjusted, as too much light can destroy the fluorescent molecules and significantly adds to fading.

(Table 4) lists the used fluorophores with the corresponding laser lines of the Leica TSP2 microscope.

**Table 4: Fluorophores and Wavelenghts**

| Fluorophore | Excitation λ [nm] | Emission λ [nm] | Exciation Laser Line [nm] |
|---|---|---|---|
| Alexa Fluor 488 | 490 | 523 | 488 |
| Atto 633 | 633 | 647 | 631 |
| Cy2 | 476 | 518 | 476 and 488 |
| Cy3 | 544 | 637 | 543 |

### 2.2.2 Deconvolution

Deconvolution is a term in optics that is specifically assigned to the process of correcting optical errors and image aberrations. It can lead to better and clearer images, enhancing the resolution and intensifying contrast. Image sharpening is also often associated with deconvolution, as it can correct the errors of a blurred image that resulted from motion during capturing. Images that are flawed from optical problems like a flawed lens can also be corrected. For the method to work one usually assumes that light travels through the microscope in a perfect way but is then convoluted with a point spread function (PSF), which distorts the image and thus describes how these distortions work in mathematical terms (Cheng, 2006).

If the PSF could be measured, then theoretically it is just a simple matter of computing its complementary function and the image would be aberration free. In practice it is not possible to obtain the true PSF, so an approximation is used that can be calculated theoretically (Nasse and Woehl, 2010) based on experimental estimation by using known probes. The accuracy of the PSF will then dictate the final result.

If the true PSF is unknown, it is still possible to do deconvolution (called blind deconvolution) by trying different PSFs and checking if the image quality has improved. This is usually done in astronomy where most images consist only of point sources (the stars) and thus the PSF can be generated from the images. In fluorescence microscopy it can be used to separate

multiple unknown fluorophores, but it is always better to gather some experimental data and try to calculate a PSF base on these data (Cheng, 2006).

In a mathematical example, the Fourier deconvolution is the converse of the Fourier convolution in the sense that division is the converse of multiplication. In practice, two signals can be deconvolved by point-by-point division from another in the Fourier domain. Afterwards one has to inverse-transform the result to the original domain again. (O'Haver, 2016).

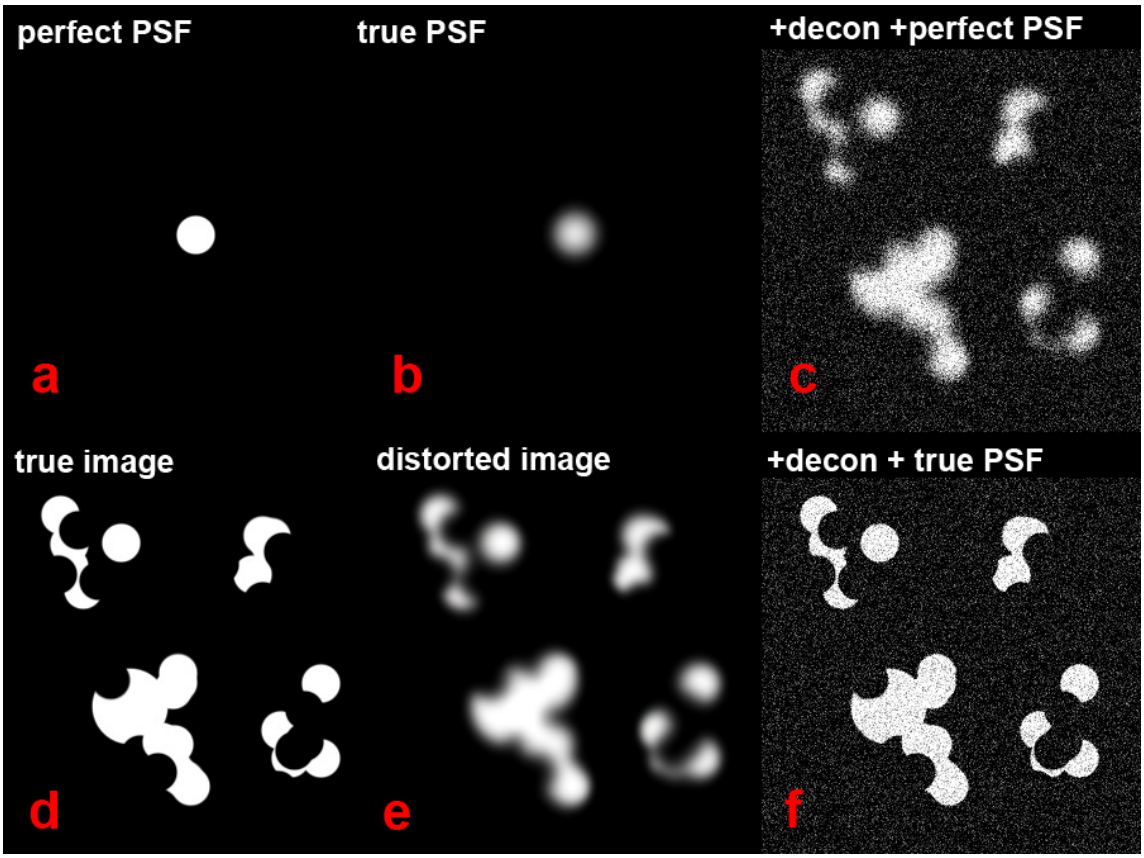


**Figure 10: a) undistorted PSF (not to scale) of a point source b) blurred PSF, contrast and sharpness is lost c) the deconvoluted image, but with a wrong PSF. So no image restoration was possible and additional noise was introduced. An example of how deconvolution can go wrong if one is not careful. d) the original light information that we want to image e) the distorted image that is observed for example through the microscope f) the deconvolved image using image e deconvolved with the PSF from b. sharpness and contrast is again excellent but additional noise is introduced.**

The process of the image formation by a convolution can be described in equation form

**e = b * d**

The letters are referring to the images above. So the image **e** is a product of the real light (information) in **d** convoluted ( ***** the convolution operator implies an integral over the space) with the PSF in **b**.

So if convolution is the replacement of every original light source with its correspondent PSF to get a blurry image, the opposite way would give us a sharp image, collecting all the spread out light and putting it back to its place. In a real case the photon noise must also be taken into account so there is another variable to the equation. As the photon noise cannot be perfectly measured, one always introduces a little bit of noise with the deconvolution and the perfect restoration of the image is not possible (see Fig. 10).[1]

The program that was used for deconvolution is **Huygens Essentials** by Scientific Volume Imaging B.V, Netherlands.[2] It uses simple wizards so those users who are unfamiliar with the area of image deconvolution still can use it to great effect. As we didn't want to do blind deconvolution we used fluorescent nano particles (PS-Speck™ Microscope Point Source Kit). These particles have a defined size of 175 nanometers and are therefore close to the resolution limit of the confocal microscope. The sample preparation and imaging for this kit was done the same way that is done with the normal biological samples, thus ensuring that one gets the best correlation between the PSF on the particles and on the real images. In the case of the PS-Speck Kit dilution of 5 µL of the content with 5 µL of distilled water and pipetting it on the microscope slide resulted in a concentration suitable for imaging at the highest magnitude of the microscope.

[1] https://svi.nl/HuygensDeconvolution, February 2016
[2] https://svi.nl, February 2016

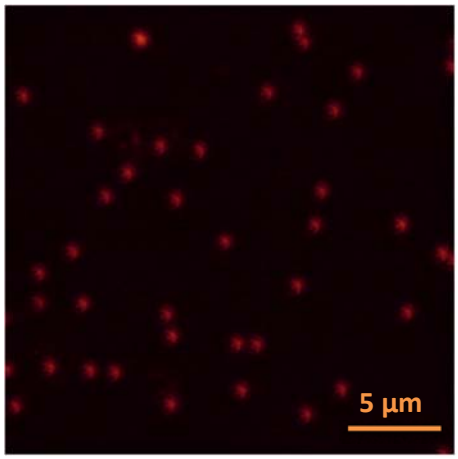


To get the correct PSF one has to image a whole image stack of the point sources (Fig. 11) and use the PSF wizard in Huygens Essential. The acquisition parameters for the stack have to be the same as for the image stacks of biological samples.

**Figure 11: sample image of one plane of the PS-Speckles. They should be perfect points without distortion from the microscope.**

As can be clearly seen in (Fig. 12), the PSF obtained from and image stack of fluorescent particles is quite distorted and would resultin a blurred image if left uncorrected.


**Figure 12: PSF generated by the PSF distiller wizard in Huygens Essential. Distortion is clearly visible.**

For deconvolution it is important to consider the used objective and several other parameters. Maximum and minimum zoom factor is the most important parameter that has to be adjusted in the imaging software, as it will determine if the image is under or oversampled. For undersampled images (not enough zoom – less detail) deconvolution is not possible. Oversampling should be avoided as that can lead to severe bleaching of the sample (see Table 5).

**Table 5: used objective parameters for the LEICA SP2 CLSM**

| **Objective** | **20x air** | **50x water** | **63x oil** |
|---|---|---|---|
| ***numerical aperture*** | 0,5 | 0,75 | 1,4 |
| ***lateral resolution [nm]*** | 434,4 | 289,6 | 155,14 |
| ***Nyquist frequency at 1024x1024pixels*** | 732,42 | 293 | 232,52 |
| ***resolution / Nyquist frequency*** | 0,59 | 1,01 | 0,67 |
| ***optimal voxel size*** | 173,76 | 115,84 | 62,06 |
| ***max. zoom factor*** | 5,06 | **2,97** | **4,5** |
| ***min. zoom factor*** | 3,37 | **1,98** | **3** |

## 2.3 Electron Microscopy

The purpose of the electron microscopic experiments was to label the α-BTX binding sites with a gold marker. For this, tissue sections were incubated with α-BTX coupled with biotin, followed by incubation in streptavidin-nanogold, silver-enhancement of the gold particles and in some experiments gold toning. The sections were then post-fixed, embedded in epoxy resin, thin sectioned, contrasted, and visualised in the electron microscope. In control experiments, the NC82 antibody was used to label the Bruchpilot antigen with a nanogold-coupled secondary antibody.

Electron Microscopy posed the biggest challenge in this project, as the tissue morphology had to be well enough preserved for small features like synapses and membranes to be visible. In traditional protocols the glutaraldehyde (GA) fixation works best and was also tested in initial experiments. The main problem is that this diminishes the binding capacity of α-BTX to the nAChRs as they are no longer present in their natural state. Even at very small concentrations of 0.1% GA the binding capacity is significantly reduced (Jones et al., 2002). One possible option here are unfixed sections, were the receptor are in their native state and could be postfixed by immersion fixation with GA after the labelling is done. The downside is that unfixed sections aren't compatible with permeabilization steps so the penetration of the antibody will be poor and only receptors on the cells surface could be made visible (Jones and Wonnacott, 2004). All experiments were done with fixed slices (2% PFA), so permeabilization could be achieved with saponin. In the case of the control experiments with the NC82 antibody 0.1% GA was used in addition, giving much better overall tissue preservation.

The biggest difference between the electron microscopy protocol and the protocol used for fluorescence was that nanogold-conjugated Streptavidin was used for EM in a second incubation step (see Table 6). As nanogold particles are only 1.4nm in diameter, it is not easy to detect them in the EM. A silver enhancement step is required to grow the size to about 5-10 nm. This was done with the Nanoprobes HQ Silver Enhancement Kit in a darkroom. A problem arises with the silver, as it is not stable in the presence of osmium tetroxide. One possible solution to this problem is the reduction of the concentration to 0.1% but this

reduces the membrane contrast. The best solution is a special step, gold toning (Leitinger et al., 2000), where additional gold is deposited on top of the silver to make the particle resistant to 1% osmium tetroxide. This is done right after silver enhancement still in the darkroom. After post fixation the sections are then dehydrated using a series of ethanol and transferred to TAAB resin using propylene oxide as intermedium. The resin was cured for 3 days at 60°C.

The blocks containing vibratome sections labelled with α-BTX or NC82 were then examined light and electron microscopically. For light microscopy, semithin sections were made at 500 nm thickness, stained with toluidine blue, and visualised to identify the neuropiles.

For EM, thin sections were made at 50 nm thickness. Counterstaining of the cut sections was then accomplished with lead citrate and platinum blue and the section were visualised with an FEI Technai 20 transmission electron microscope (Table 6).

**Table 6: SOP for electron microscopy**

| | chemicals | temperature | duration |
|---|---|---|---|
| Fixation | 2% PFA, 0.1M PB, pH 7.4 | RT | 3 h |
| Rinse | Rinse in PB | 4° C | 1 h |
| embedding | Gelatine (15% in PB) | on ice | - |
| fixation | 2% PFA, 0.1M PB, pH 7.4 | 4°C | 2 h |
| rinse | Rinse in PB | 4° C | ON |
| cutting | Cut 70µm sections with vibratome | 4°C | - |
| storage | Transfer to PBS | 4°C | - |
| prepare PBG | 0.05% Saponin, 0.8% BSA, 0.1M glycine in PBS | Store at 4°C | - |
| preincubation 1 | 0.05M glycine in PBS | RT | 10 min |
| preincubation 2 | 5% normal goat serum in PBG | RT | 30 min |
| incubation | Incubate overnight with 10nM bungarotoxin in PBG | 4°C | ON |
| rinse | 3x PBS | RT | 3x10min |
| incubation | Incubate in streptavidin-nanogold 1:100 | RT | 4 h |
| rinse | 3x PBS | RT | 3x10 min |
| postfix | 2% PFA/2.5% GA in 0.1M PB | RT | 30 min |
| rinse | 3x PBS | RT | 3x10 min |
| wash | 20mM citrate buffer 7.0 pH | RT | 3x5 min |
| HQ silver | 3 drops Solution A/B/C. | RT | 3 min |

| | | | |
|---|---|---|---|
| | Darkroom! | | |
| Rinse | 150 mM $NaNO_3$ | RT | 5 min |
| Gold toning | 0.05% Tetrachloroauric[III]acid in 150 mM Acetate buffer, 5.6pH | RT | 7 min |
| Rinse | 150 mM $NaNO_3$ | RT | 2x5 min |
| wash | PB | RT | 2x10 min |
| storage | PB | 4 °C | ON |
| postfix | 1 % osmium tetroxide (see Table 9) | RT | 30 min |
| wash | PB | RT | 2x10 min |
| dehydration | Series of ethanol (appendix) | RT | varies |
| embedding | TAAB epoxy resin (see Table 8) | 60 °C | 3 days |
| counterstain | Lead citrate and platinum blue | - | - |

**Table 7: stock solutions for PBG and PBG recipe for 100mL**

| | prepare stock solution | for 100ml PBG | end concentration |
|---|---|---|---|
| 5% Saponine in PBS | 0.5g in 10mL | use 1mL of stock | 0.05% |
| 10% Fish Gelatine | 1:5 in 10mL | use 1mL of stock | 0.1% |
| 0.1M Glycine | | use 0.75g | 0.1M |
| 0.8% BSA | | use 0.8g | 0.8% |

PBG (Table 7) had to be prepared fresh for every new experiment, If one does multiple experiments week after another then also 0.02% sodium azide can be added as to prevent fungus growth. Table 8 and 9 show the recipes for TAAB resin and osmium tetroxide preparation.

**Table 8: ingredients for TAAB**

| | |
|---|---|
| TAAB epoxy resin | 50 parts |
| DDSA | 25 parts |
| MNA | 25 parts |
| DMP-30 | 2 parts |

**Table 9: osmium tetroxide preparation**

| | |
|---|---|
| $OsO_4$ 1% | 1 parts |
| *dd*$H_2O$ | 1 parts |
| Phosphate buffer | 2 parts, 0.2 M |

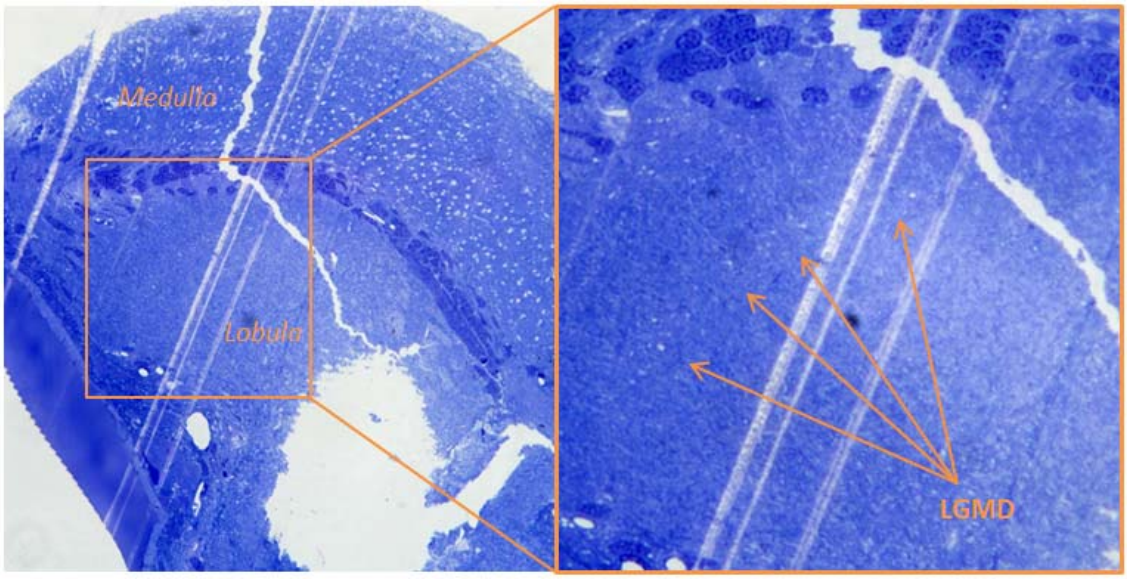


**Figure 13: left: semi-thin section of the optic lobe, lobula complex and medulla are easily discernible. right: detail of the lobula where the LGMD is visible.**

Orientation is crucial to finding the LGMD in the cut sections. Semi thin sections are often confusing, as only a part of the *lobus opticus* is visible. The best approach is to look for the medulla as it has a very specific pattern of small round white cells in the toluidine staining and, once the medulla has been identified, to search for the lobula complex. The semi thin section in (Fig. 13) was a lucky section, as it contains the lobula complex and medulla at the same time. More often than not only a very small part of either was visible, due to the distortion and curling of the sections during dehydration in ethanol. To circumvent this problem we tried to fix the sections between cover slips but it did not have any impact, it poses also the risk of breaking the brittle sections.

Under the light microscope the LGMD 1 and 2 in the lboula complex can be identified by their double structure. Within the dorsal lobula complex, there are two semi-circular crescents of LGMD dendrites, one belonging to the LGMD 1 and the other to the LGMD 2. They have a curved shape following roughly the curvature of the lobula complex. Identification for 100% can only be done under the electron microscope where a characteristic arrangement of afferent neurons along the LGMDs' dendrites becomes visible: characteristically, the afferent neurons are presynaptic to the LGMD and to each other.

# 3. Results

The most important results of this thesis were the establishment of suitable protocols for labelling nicotinic acetylcholine receptors for Fluorescence and EM. These protocols are printed in the appendix. The optimization of those steps was critical. There is always room for improvement, for example identifying specific neurons on thin sections that had been labelled for $\alpha$-BTX proved extremely time consuming and was beyond the scope of this thesis. I will address this in the discussion.

Fluorescence microscopy was a great tool for learning to handle the locust tissue and getting to know the anatomy of the locust's optic lobe. The first experiments showed that from using fluorescently labelled $\alpha$-BTX to label nAChRs, a distinctive staining pattern in the lobula complex can be gained. Closer inspection of overviews of the dorsal lobula complex showed that in the area were the LGMD's dendrites should be located, there is increase in fluorescence in a semi-circular pattern around (Fig. 15 A). A comparison with a published section of the same orientation containing a Golgi silver stain of the LGMD 1 (Fig. 15 B) showed that these semicircles are likely to be the location of the LGMD's dendrites, and the bright fluorescence originates from highly concentrated nAChRs at their cell membranes.

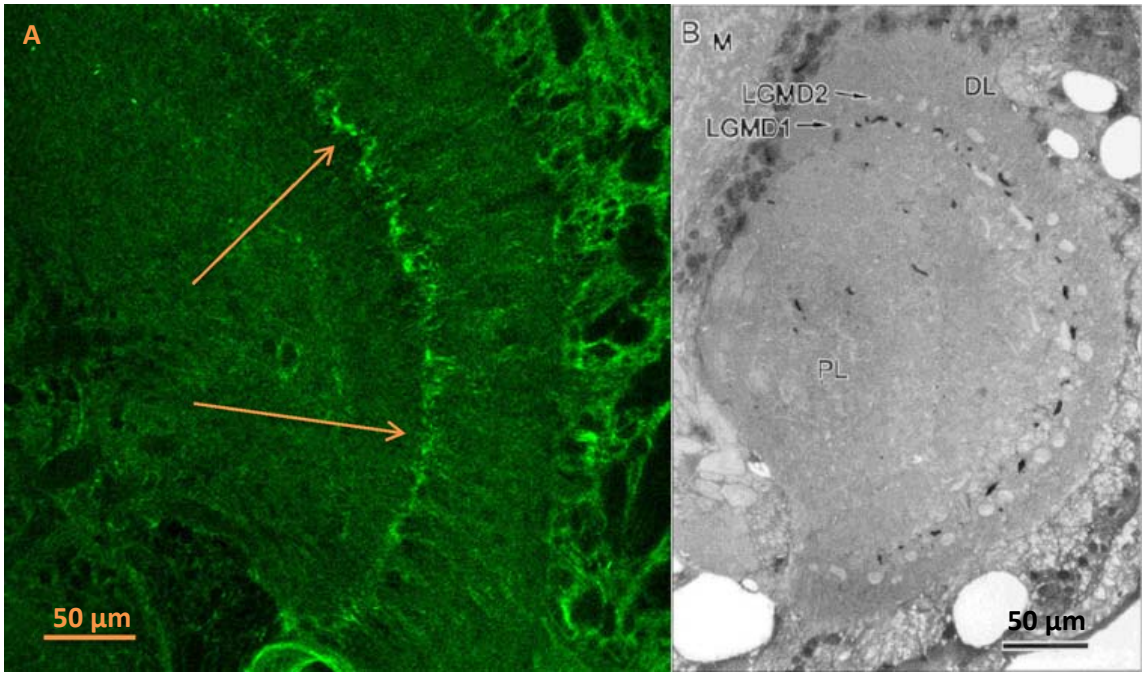


**Figure 14: (A) CLSM image (20x objective magnification) of the lobula complex with bungarotoxin coupled to Alex Fluor488 in the green channel. Arrows point to areas of most prominent staining, possibly the LGMD's dendrites (B) silver staining of the lobula complex with LGMD 1 and 2 shown. (Rind and Leitinger, 2000); DL: distal lobula, PL: proximal lobula, M: Medulla**

Generally speaking, the fluorescence is very high in the whole lobula complex and there are not many blank spots, so it would appear that the nicotinic receptor is universally expressed there.

## 3.1 Fluorescence Microscopy

### 3.1.1 Testing deconvolution and visualizing the LGMD

For fluorescence microscopy at intermediate and high magnification, it was important to test the effect deconvolution would have on our acquired images. As can be seen in (Fig. 15); contrast, sharpness and signal to noise ratio greatly improved by using the deconvolution wizard in Huygens Essential. I want to emphasize here that deconvolution is something that has to be considered before image acquisition as it needs special acquisition parameters to work.

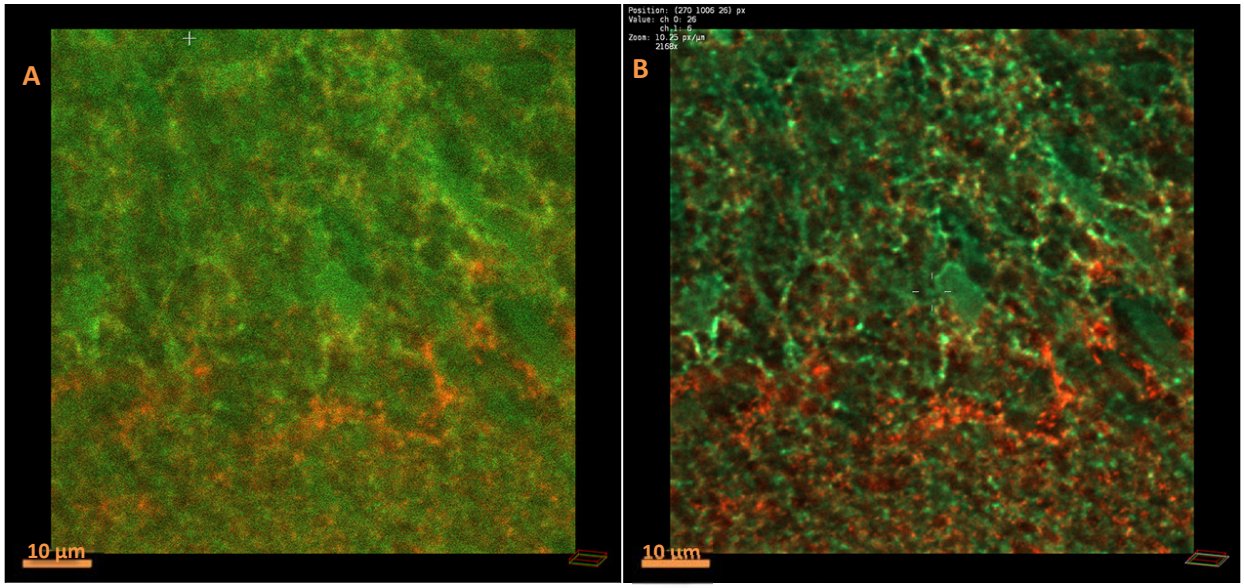


**Figure 15: (A) comparison between a CLSM image without deconvolution (B) same image with deconvolution in Huygens Essential. Both images are visualized at the same time with the Huygens Twin Slicer tool. Red: bungarotoxin, green: Nc82 antibody. 63x objective, zoom 4.5**

The parameters that were universally used with all the images are shown in (Fig. 16). The most important one is the signal to noise ratio, as Huygens Essential performs both denoising and deconvolution and this parameter is used to assess the noise level in the original images. If this parameter is set too high, the deconvolution process results in exaggerated sharpening of the image and tiny artefacts become visible. Experiments with lower numbers should be made if such artefacts appear in the deconvolved image.

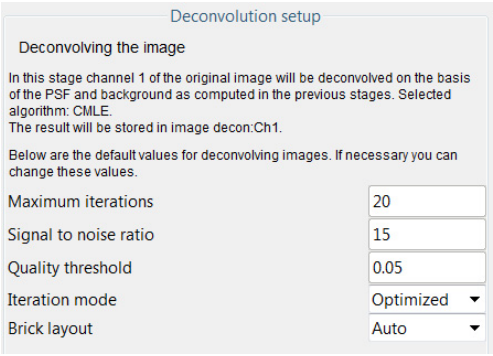


**Figure 16: Deconvolution setup in Huygens Essential, these parameters were used with all following images**

Because the LGMD was more intensely labeled with α-BTX than its surround, I was able to visualize it using α-BTX labelling (coupled with either Alexa Fluor 488 or with Atto633 fluorescent dyes). For this, image stacks were acquired at an intermediate magnification (50x water objective). These image stacks are useful as they allow tracing the cells inside the tissue (Fig. 17 A).

There is the option in Huygens Essential to do a 3D animation film of a CLSM image stack, This was great for visualizing the finger-like-dendrites of the LGMD 1 and 2 (Fig. 17 B).

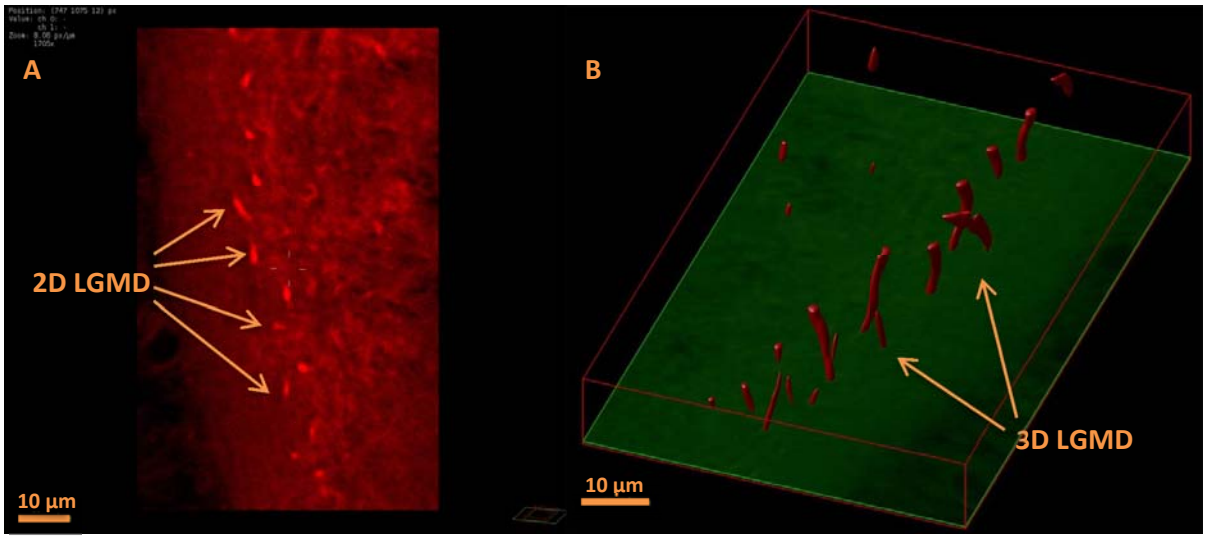


**Figure 17: (A) Single image of a CLSM Stack used to generate a 3D Animation of the whole stack. (B) Single Image out of an animated Avi-film that shows the LGMD 1 and 2 arms in the imaged CLSM stack. Depth of the stack is approximately 10µm. Red signal: α–BTX. 50x Objective Magnification**

### 3.1.2 Fluorescence double labelling with NC82 antibody and bungarotoxin

By performing a double labelling experiment with both α-BTX and NC82 antibody, co-localization of nicotinic acetylcholine receptors and bruchpilot protein was addressed. In this experiment both antibodies were applied at the same time overnight. As bungarotoxin is coupled to a different fluorophore than NC82 they were then detected separately. Fig. 18 A shows the reaction of bungarotoxin (green) in the dorsal lobula, whereas Fig. 18 B shows the reaction of NC82 (red) on the same section, scanned at high magnification. Both the dendrites of the LGMD 1 and the dendrites of the LGMD 2 were visible as blank spots surrounded by ring-like fluorescence of both markers, due to the fact that nicotinic acetylcholine receptors are situated at the cell membrane of the LGMD's dendrites, and the presynaptic bars surrounded the dendrites. Strikingly, the α-BTX labelling surrounding the LGMD 1 was much stronger than the NC82 labelling surrounding this neuron, whereas the NC82 labelling surrounding the LGMD 2 was much stronger than the α-BTX labelling surrounding the LGMD 1 (compare Fig. 18 A and B). This implies that labelling at the LGMD 2 is stronger with bungarotoxin, and at the LGMD 1 with NC82 antibody, but there is also quite good labelling at the LGMD 1 with bungarotoxin.

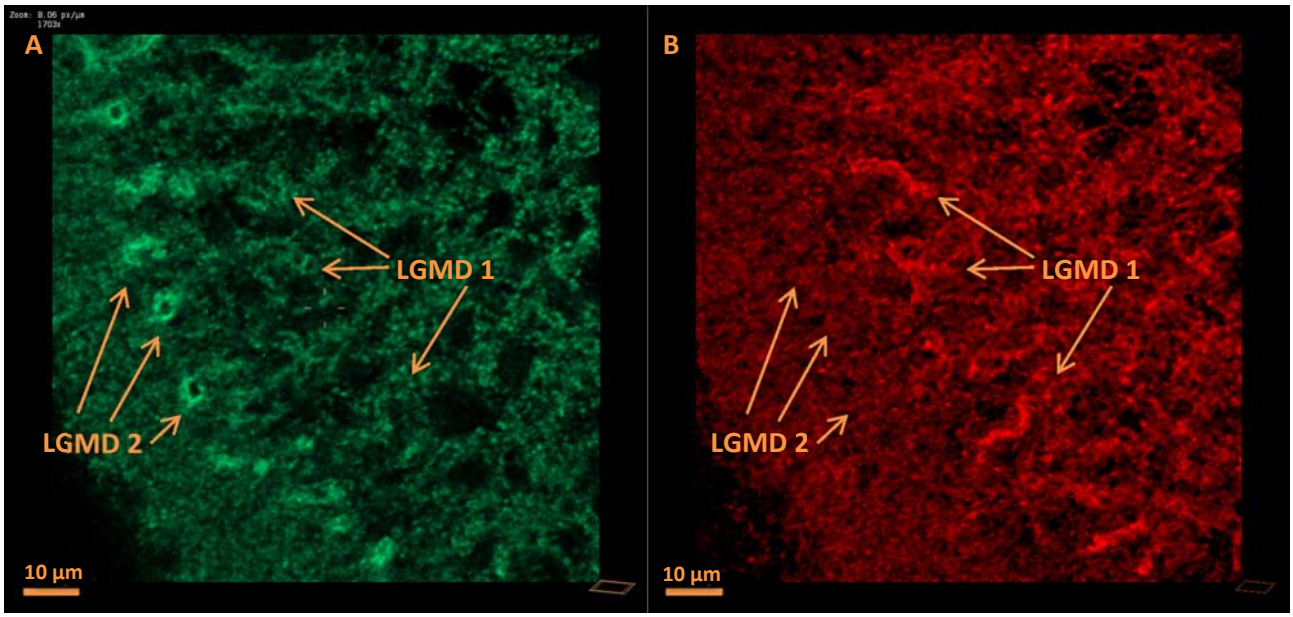


**Figure 18: CLSM image, Red: NC82 antibody, Green: Bungarotoxin. In (A) there is LGMD 2 visible, the structure in (B) is supposed to be LGMD 1. All arrows in the images are pointing at the same locations in both images. Made with Huygens Essential Twin Slicer tool. 63x objective magnification, zoom factor 3.**

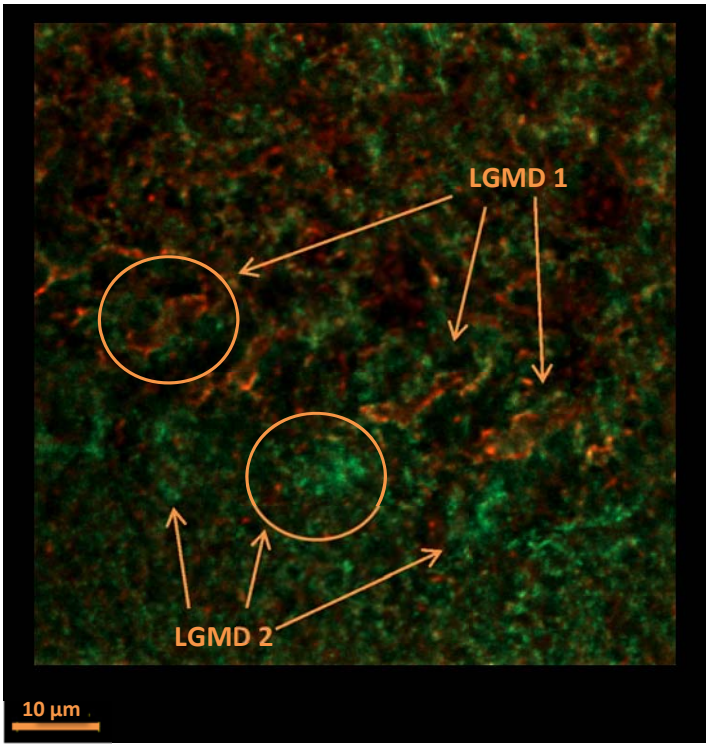


**Figure 19: CLMS image, Lobula complex, Green: bungarotoxin, Red: NC82 antibody. LGMD 1 shows very good colocalization while at the LGMD 2 there is an abundance of bungarotoxin labelling. 63x objective magnification, zoom factor 4.5**

An overlay and detail image with even higher zoom factor (Fig. 19) shows that at the LGMD 1 there is clear co-localization but at the LGMD 2 the bungarotoxin binding is so strong that the NC82 signal is not seen anymore. This special pattern has been consistent over all detail images that were taken from the LGMD area. This might be due to binding of $\alpha$ -BTX to GABA receptors (Hannan et al., 2015) which are only expressed in the area of the LGMD 2 (Rind and Simmons, 1998). This would make it more complicated to reliably label nAChRs in the future, as one has to be sure that there are no GABA-receptors in the vicinity of them.

## 3.2 Electron microscopy

For labelling α-BTX at EM level, a working protocol could be established. As first results were all negative, different changes to the protocol were introduced and a test was performed with NC82 as a positive control using a previously published protocol (Leitinger et al., 2012) if sample preparation was done in the right way. For the final protocol please see the methods section and the appendix.

### 3.2.1. Osmium tetroxide concentration test

As Osmium Tetroxide is a problem for the silver enhancement step that was needed to visualize the small nanogold particles (Leitinger et al., 2000), one experiment was to lower the osmium tetroxide concentration to 0.1% and compare it with 1%.

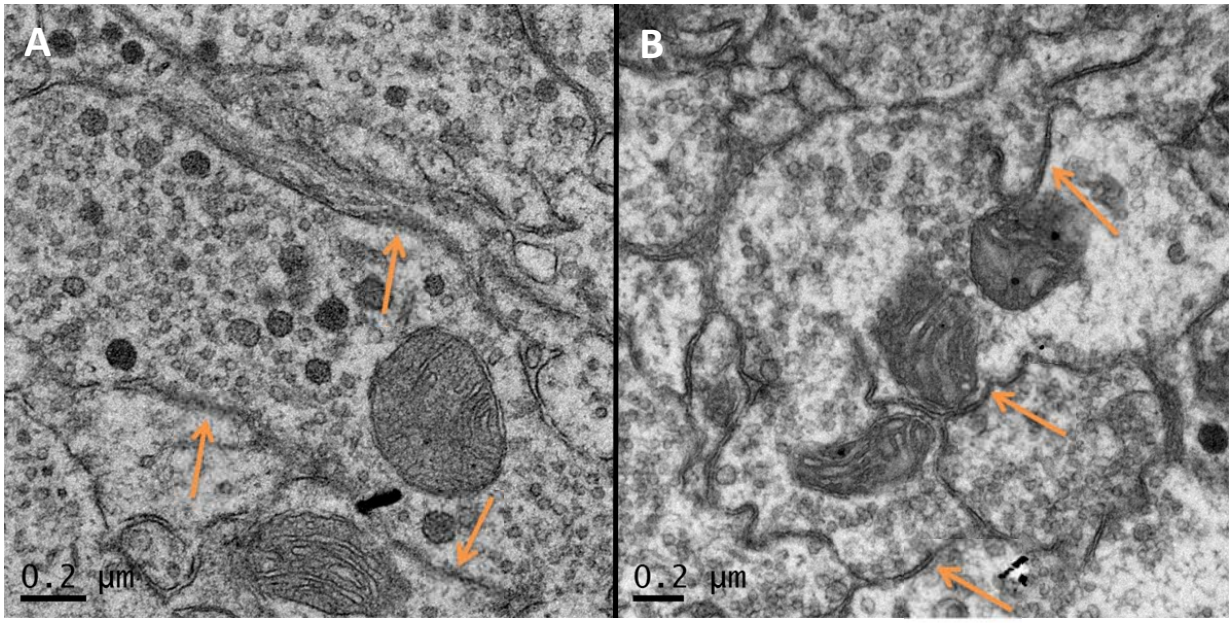


**Figure 20: difference between (A) 0.1% osmium tetroxide versus (B) 1% osmium tetroxide. Arrows are pointing at membrane spots with bad contrast in image (A) and very good contrast im image (B)**

Lower concentration leads to weaker staining and membrane contrast is general low (Fig. 20 A). In my opinion the higher concentrated osmium (Fig. 20B) results in overall better images that are easier to look at when searching for details like synapses. The downside is that 1% osmium attacks the silver that is deposited on the gold particles (see also (Leitinger et al.,

2000)), so a gold toning step was performed after silver amplification. Silver is exchanged with gold in this step, which results in gold particles that withstand 1% osmium tetroxide.

### 3.2.2. Labelling of Bruchpilot protein by the NC82 antibody

The first positive immunolabelling result was achieved with the NC82 antibody in conjugation with 1% osmium tetroxide postfixation and gold toning. The protocols were adapted from (Leitinger et al., 2000, 2012). After fixation (with GA) and sectioning, the sections were incubated with the NC82 antibody followed by streptavidin-nanogold. To enhance the nanogold, HQ Silver enhancement Kit (3 minutes per section) with gold toning was performed. After dehydration and postfixation the sections were then embedded in TAAB resin.

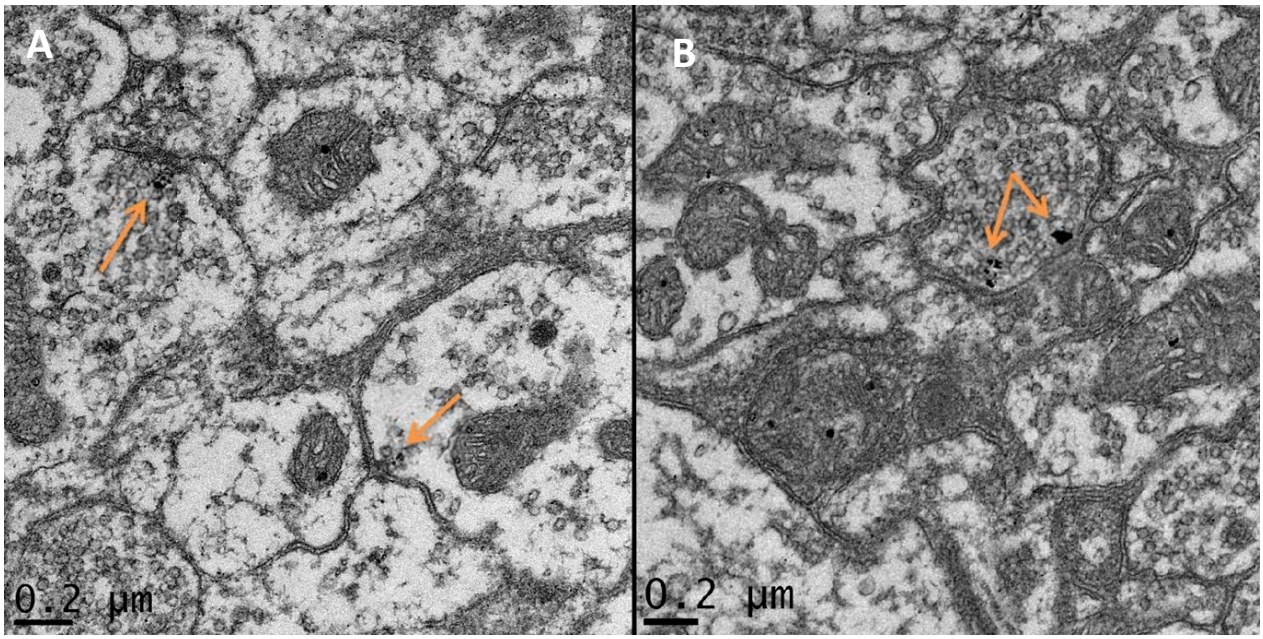


**Figure 21: NC82 labelling, arrows point to the silver particles and in the direction of the synapse with its neighbouring cells. (A) the silver particles are presynaptic at the site of the vesicles (B) two synapses in one cell containing a lot of neurotransmitter vesicles.**

In (Fig. 21) one can see the immunogold labelling of the presynaptic bruchpilot protein. It is involved in the anchoring of vesicles to the active zone. Membrane contrast is very good and the neurotransmitter vesicles conservation is also easy to be seen.

### 3.2.3. Differences in tissue preservation without GA

The protocol from the NC82 labelling was also used to compare the tissue preservation with and without GA in the first fixative. These were not separate experiments but observations from several experiments I have done while trying to get the immunohistochemistry to work.

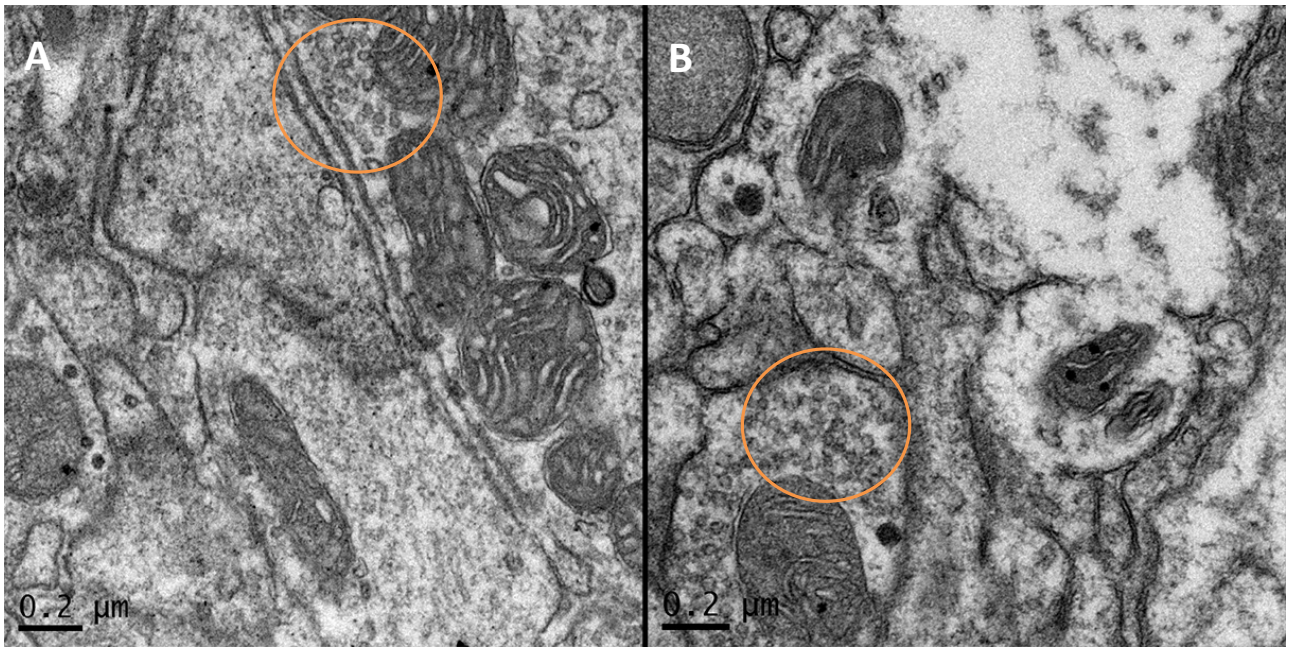


**Figure 22: direct comparison between EM sections treated with/out GA (A) no GA (B) with 0.1% GA. Neurotransmitter vesicles are designated in a circle.**

With (Fig. 22) I would like to emphasize the effect that the missing GA has for the fixation of the tissue: preservation of fine structure is less good when GA is omitted in the first fixation step (Fig. 22 A) than when it is included (Fig. 22 B). The effect is most notably on the cell membranes and could be a problem for identifying synapses. Vesicles are easily identifiable in both images.

### 3.2.4. Labelling of nAChRs with α-BTX

Once a working immunohistochemistry protocol for NC82 labelling was established, it had to be adapted for labelling α-BTX. Mainly, GA had to be excluded from the first fixative as α-BTX does not bind to GA-fixed nicotinic acetylcholine receptors (Jones and Wonnacott, 2004).

After fixation (without GA) and sectioning, the sections were incubated with α-BTX followed by streptavidin-nanogold. To enhance the nanogold, HQ Silver enhancement Kit (3 or 6 minutes per section) with gold toning was performed. After dehydration and postfixation the sections were then embedded in TAAB resin. This protocol clearly resulted in distinct labelling of α-BTX in unidentified neurons of the lobula (Fig. 23). The question whether the protein is localized pre or post-synaptically to the LGMD could not be answered, as the LGMD couldn't be located in these sections. Membrane contrast was good (due to 1% osmium tetroxide and gold toning) but overall tissue conservation was not as good as with GA fixed perfused sections. It was however good enough to see features like synaptic densities and neurotransmitter vesicles and the labelling in (Fig. 23 B) is in the vicinity of those vesicles.

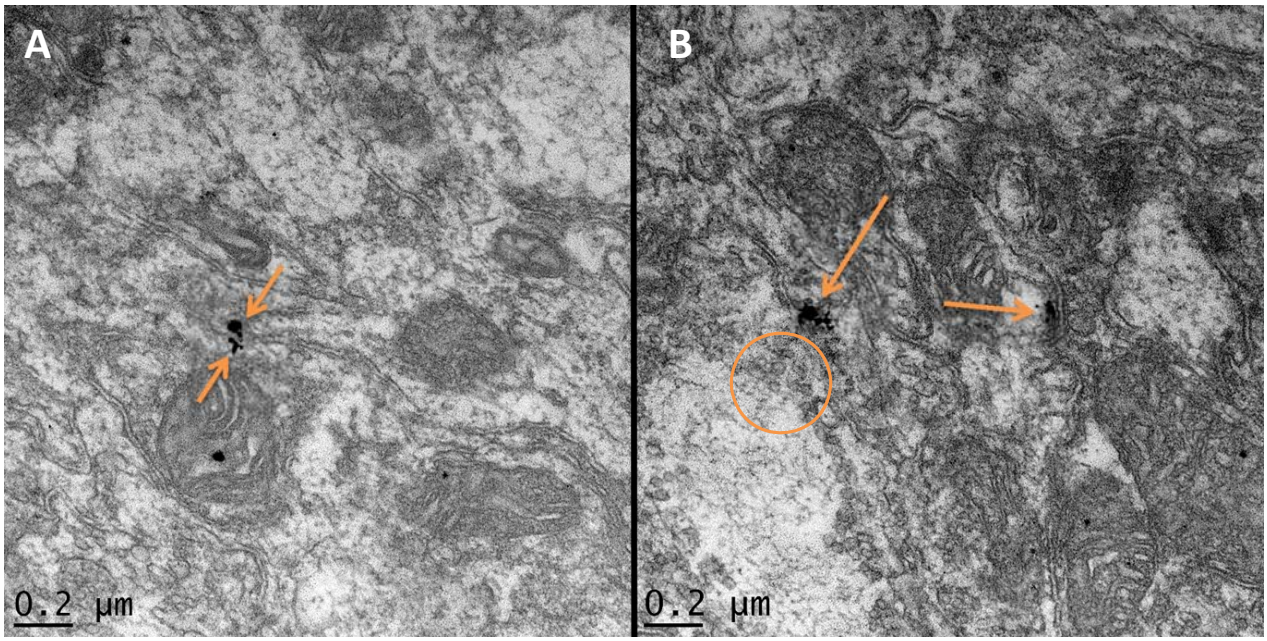


**Figure 23: α-BTX labelling, showing not quite as good membrane resolution due to the missing GA fixative. (A) would suggest that the receptors are found pre and postsnaptically (B) would suggest that the receptors are found postsynaptically. The orange circle shows neurotransmitter vesicles in the vicinity of labelling**

### 3.2.4. Localization of the LGMD in the EM

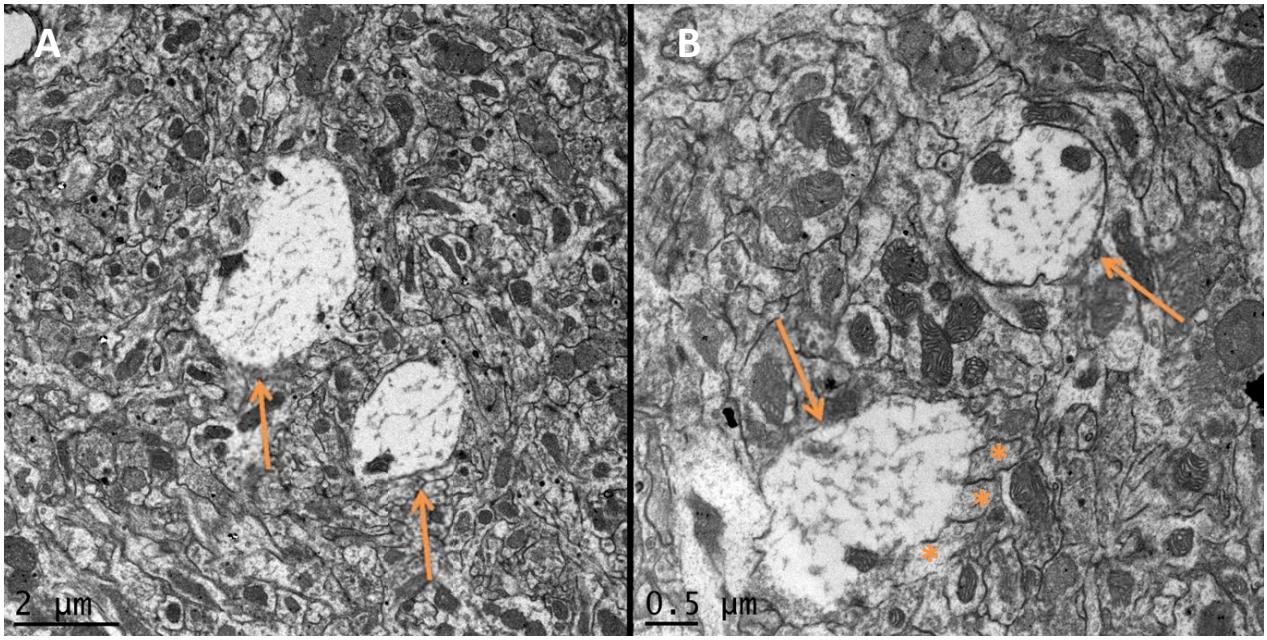


**Figure 24: LGMDs indicated by the orange arrows in the *lobula complex* by TEM, (A) they are best identified at lower magnifications (B) higher magnification showing afferent cells (*)**

Localization of the LGMD (Fig. 24 A) worked in one of the earlier protocol runs; unfortunately no labelling is present in these sections as GA was used as a first fixative. The main feature for detecting the LGMD in the TEM is that the cell is in general very bright and without neurotransmitter vesicles as there are no output synapses present. In general it is surrounded by many smaller cells, the TMAs which form reciprocal synapses with the LGMD and neighboring TMAs (Fig. 24 B). Also there should always be other LGMD dendrites nearby, so if one cell is found the next should not be too far away.

# 4. Discussion

In this thesis, the protocol for detection of nAChRs in the locust's optic lobe with both CLSM and EM was established and both the α-BTX labelling and the NC82-labelling surrounding the LGMD dendrites were studied in detail light microscopically. This thesis will be useful as a starting point for detection of any other proteins in the locust's tissue with these two methods.

Several experiments had to be performed to get to the necessary optimization of the protocols right. Initial setbacks and pitfalls took time to get rid of. With the CLSM this included the right orientation of the sections during vibratome sectioning and learning how to use the microscope at a level that no photo bleaching did occur. Also the issue of non-binding antibodies (or expired fluorescent dyes) had to be solved.

At the EM level the problems were manifold more, at first it looked like the silver enhancement step was the critical problem but it then was shown that the orientation and finding of the LGMD was the biggest challenge after the working protocol was established.

## 4.1 Methodical insights

The first question was: Can the nAChRs in the synapses of the lobula complex be labelled? After literature search the idea of using α-BTX was born, but it could not be predicted if it would work in the locust (Young et al., 2003) as it had been shown to label nAChRs in the rat (Jones and Wonnacott, 2004). Before wasting precious time with time consuming electron microscopy, I chose confocal laser scanning microscopy for a relatively easy way to test if there would be a positive signal. First results were all positive and as there was also a distinct α-BTX staining pattern in the area where the LGMD is located.

From other experiments, I was able to show that it is possible to identify the LGMD's dendrites in the outer lobula complex from vibratome sections that were embedded in epoxy resin. Careful orientation and pre-selection of section containing the outer lobula was necessary for this. Furthermore, the LGMD had to be identified first on semi thin sections in the light microscope and second on thin sections taken from the same block in the EM. A similar procedure had been successful earlier for vibratome sections labelled with synapsin-

gold (Leitinger et al., 2004). The localisation of the LGMD cell is tricky when the sections are not perfectly flat, making it difficult to orient them during ultramicrotomy. The sections are almost never flat as the dehydration process in the ethanol curls them. A solution of this problem would improve the whole workload. Many sections that are fixed just do not contain the LGMD at all, as this cell is only 150 µm in overall length. A reliable method to check for the cell at light microscopy level would be needed to relief the workload of looking at sections with no relevant information to the experiment. There is also the problem that the antibody in these experiments only binds within 10-20 µm of the surface of the 70 µm thick section and the LGMD is only 150 µm in length. So at a maximum of three sections out of about 20 sections cut with the vibratome there will be a part of the LGMD present. Most of the sections used in immunohistochemistry yield no information for the experiment but this can only be confirmed by cutting them with the ultra-microtome and thus requires a lot of time.

Because of the high workload for labelling for EM and identifying the LGMD, combining successful α-BTX labelling and identifying the LGMD's dendrites proved beyond the scope of this thesis. This will be necessary for showing the EM distribution of α-BTX around the LGMD's dendrites. One step further here would be to try the PLP-fixative to increase the labelling density (Hall et al., 1987) that is recommended for immunostaining with cryostat sections, this was also used in (Jones and Wonnacott, 2004) in conjunction with α-BTX.

## 4.2 Insights on the results

I demonstrated light microscopically that we can find labelling for bruchpilot protein and NAChRs around the LGMD-dendrites. This is conform with the theory (Rind and Leitinger, 2000; Jones and Gabbiani 2010) that the synapses are cholinergic.

α-BTX labelling was high throughout the lobula neuropile and especially high amount of α-BTX labelling was found in the area of the LGMD 2 dendrites. The LGMD is surrounded by GABA-containing neurites (Rind and Simmons, 1998), which are absent close to the LGMD 1 dendrites in the area examined here. This leads to the thought that there may be cross reactions of α-BTX with another receptor, like the GABA-receptors. Current literature (Hannan et al., 2015) suggests that this might indeed be the case. If one wants to further

study the nAChRs with bungarotoxin then it must be in an area with no GABA receptors present (like at the LGMD 1).

Nevertheless, the fluorescent images show wide labelling of α-BTX in the lobula complex neuropile. This includes the immediate surroundings of the LGMD 1 dendrites, where no GABAergic synapses are expected. This suggests that these receptors may also be expressed on the cell membranes of TMAs. They could play a role in the reciprocal synapses between TMA cells. For this discussion, EM labelling of α-BTX surrounding the LGMD dendrites and labelling of the mAChRs would be helpful, as these should be at different locations than the nAChRs. The M35 antibody could be a starting point for the mAChRs (Carsi-Gabrenas et al., 1997) as it has been shown to label mAChRs in mammals and the moth *Manduca sexta* (Torkkeli et al., 2005).

### 4.2.1 Alternative model for the reciprocal synapse

Because my findings suggest the presence of nAChRs at the cell membrane of TMAs, in (Fig. 25) I propose a model of the reciprocal synapse, modified to show also presynaptic and preterminal NAChRs as well as possible interactions with the neurotransmitter particles. The model of negative feedback mentioned (Thany and Tricoire-Leignel, 2011) is an interesting one, as it involves nAChRs at the presynaptic site or even further at preterminal sites in the cell membrane. This could modify transmitter release if the receptors act as autoreceptors (Blagburn and Sattelle, 1987; Breer and Knipper, 1984). There is also the possibility that preterminal receptors or non-synaptic nAChRs receptors further away from the synapse have an influence on the cells' ability to release neurotransmitters (Vizi and Lendvai, 1999).

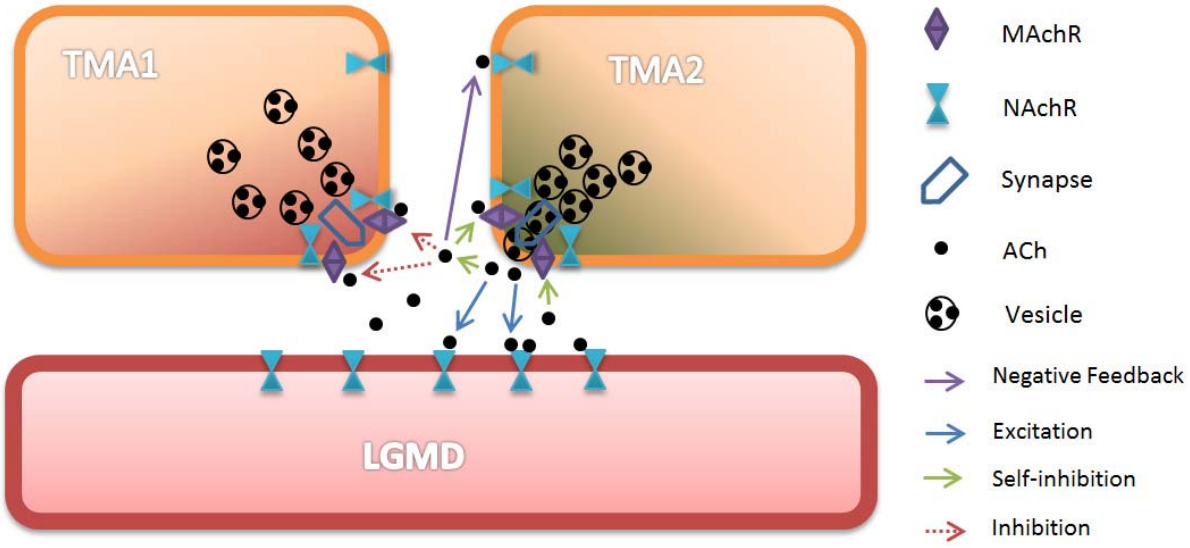


Figure 25: model of the reciprocal synapse modified after (Thany and Tricoire-Leignel, 2011).

A review about presynaptic nicotinic Ach receptors is presented in (Wonnacott, 1997), where it is questioned whether these receptors serve a physiological function after all.

If the precise localization of all the receptors involved in this system could be shown, it would us finally give the knowledge how the action at the synapse level contribute to the mechanisms of motion detection in the locust. The present work gives a basis for such future experiments.

## 4.2 Conclusions and outlook

This study proves that nicotinic receptor localization in the locust can be done with the electron microscope and it is therefore the most suitable tool if high resolution is needed. If a working protocol is already established and the localization of the area is not any longer of concern one could use electron-tomography to localize the protein in 3D tomograms. This would give the best resolution available today and will ultimately lead to a new way of seeing the importance of the proteins localization in the three dimensional system that a synapse is. To fully understand the forces at work one would also need to locate the mAChR at the same time, possible with another reaction product like DAB which can be detected alongside immunogold and make it possible to simultaneously label two proteins in the EM.

My results in this field indicated that bungarotoxin doesn't bind specifically to nAChRs, there was just too much labelling in the optic lobe. After literature search and finding the new paper (Hannan et al., 2015) my thoughts are now that we see GABA labelling as well by using this toxin. If one wants to further study the nAChRs with bungarotoxin then it must be in an area with no GABA receptors present (like at the LGMD 1).

Another promising technique in this field of work would be the ATUMtome[3], an automatic tape collecting microtome with array tomography. It would make it easier to locate the sections with the LGMD, as no sections are lost during cutting and no preselection has to take place. After sectioning, post embedding immunohistochemistry could be performed with the sections that contain the area of interest both at the light microscope and electron microscope level.

[3] http://www.rmcboeckeler.com/ATUMtome/, March 2016

## Table of abbreviations

| | |
|---|---|
| DAB | 3,3'-Diaminobenzidine |
| EM | electron microscope |
| GA | Glutaraldehyde |
| LGMD | Lobula Giant Movement Detector |
| mAChRs | muscarinic acetylcholine receptors |
| nAChRs | nicotinic acetylcholine receptors |
| Overnight | ON |
| Pb | Phosphate buffer |
| PBG | phosphate buffered saline with glycine |
| PBS | phosphate buffered saline |
| PFA | paraformaldehyde |
| PSF | Point Spread Function |
| RT | room temperature |
| Sol1 | Solution1 |
| TMA | trans-medullar afferent cell |
| $\alpha$ -BTX | alpha-bungarotoxin |

## Index of literature


Benson, J.A. (1992). Electrophysiological pharmacology of the nicotinic and muscarinic cholinergic responses of isolated neuronal somata from locust thoracic ganglia. J. Exp. Biol. *170*, 203–233.

Blagburn, J.M., and Sattelle, D.B. (1987). Nicotinic acetylcholine receptors on a cholinergic nerve terminal in the cockroach, Periplaneta americana. J. Comp. Physiol. A *161*, 215–225.

Breer, H., and Knipper, M. (1984). Characterization of acetylcholine release from insect synaptosomes. Insect Biochem. *14*, 337–344.

Burrows, M., and Rowell, D.C.H.F. (1973). Connections between descending visual interneurons and metathoracic motoneurons in the locust. J. Comp. Physiol. *85*, 221–234.

Carsi-Gabrenas, J.M., Van Der Zee, E.A., Luiten, P.G.M., and Potter, L.T. (1997). Non-Selectivity of the Monoclonal Antibody M35 for Subtypes of Muscarinic Acetylcholine Receptors. Brain Res. Bull. *44*, 25–31.

Chan, R.W., and Gabbiani, F. (2013). Collision-avoidance behaviors of minimally restrained flying locusts to looming stimuli. J. Exp. Biol. *216*, 641–655.

Cheng, P.-C. (2006). The Contrast Formation in Optical Microscopy. In Handbook Of Biological Confocal Microscopy, J.B. Pawley, ed. (Springer US), pp. 162–206.

Clarke, P.B.S., and Pert, A. (1985). Autoradiographic evidence for nicotine receptors on nigrostriatal and mesolimbic dopaminergic neurons. Brain Res. *348*, 355–358.

Coggan, J.S., Paysan, J., Conroy, W.G., and Berg, D.K. (1997). Direct Recording of Nicotinic Responses in Presynaptic Nerve Terminals. J. Neurosci. *17*, 5798–5806.

Denk, W., and Horstmann, H. (2004). Serial Block-Face Scanning Electron Microscopy to Reconstruct Three-Dimensional Tissue Nanostructure. PLoS Biol. *2*, e329.

Elphick, M., Williams, L., and Shea, M. (1996). New features of the locust optic lobe: evidence of a role for nitric oxide in insect vision. J. Exp. Biol. *199*, 2395–2407.

Hall, P. a., Stearn, P. m., Butler, M. g., and D'ardenne, A. j. (1987). Acetone/periodate-lysine-paraformaldehyde (PLP) fixation and improved morphology of cryostat sections for immunohistochemistry. Histopathology *11*, 93–101.

Hannan, S., Mortensen, M., and Smart, T.G. (2015). Snake neurotoxin α-bungarotoxin is an antagonist at native GABAA receptors. Neuropharmacology *93*, 28–40.

James, A.C., and Osorio, D. (1996). Characterisation of columnar neurons and visual signal processing in the medulla of the locust optic lobe by system identification techniques. J. Comp. Physiol. A *178*, 183–199.

Jones, I.W., and Wonnacott, S. (2004). Precise Localization of α7 Nicotinic Acetylcholine Receptors on Glutamatergic Axon Terminals in the Rat Ventral Tegmental Area. J. Neurosci. *24*, 11244–11252.

Jones, P.W., and Gabbiani, F. (2010). Synchronized Neural Input Shapes Stimulus Selectivity in a Collision-Detecting Neuron. Curr. Biol. *20*, 2052–2057.

Jones, I.W., Bolam, J.P., and Wonnacott, S. (2002). Localisation of neuronal nicotinic acetylcholine receptor subunits in rat substantia nigra and dorsal striatum. In The Basal Ganglia VII, L.F.B. Nicholson, and R.L.M. Faull, eds. (Jones, Ian W.; Wonnacott, Susan; Department of Biology and Biochemistry, University of Bath, Bath, BA2 7AY, UK), pp. 127–136.

Judge, S., and Rind, F. (1997). The locust DCMD, a movement-detecting neurone tightly tuned to collision trajectories. J. Exp. Biol. *200*, 2209–2216.

Killmann, F., Gras, H., and Schuermann, F.-W. (1999). Types, numbers and distribution of synapses on the dendritic tree of an identified visual interneuron in the brain of the locust. Cell Tissue Res. *296*, 645–665.

Kittel, R.J. (2006). Bruchpilot Promotes Active Zone Assembly, Ca2+ Channel Clustering, and Vesicle Release. Science *312*, 1051–1054.

Knipper, M., and Breer, H. (1989). Muscarinic receptors modulating acetylcholine release from insect synaptosomes. Comp. Biochem. Physiol. C *93*, 287–292.

Leitinger, G., Pabst, M.A., and Kral, K. (2000). Gold toning preserves integrity of silver enhanced immunogold particles during osmium tetroxide treatment for demonstration of a biogenic amine. Brain Res. Protoc. *5*, 30–38.

Leitinger, G., Masich, S., Neumüller, J., Pabst, M.A., Pavelka, M., Rind, F.C., Shupliakov, O., Simmons, P.J., and Kolb, D. (2012). Structural organization of the presynaptic density at identified synapses in the locust central nervous system. J. Comp. Neurol. *520*, 384–400.

Marshall, J., Buckingham, S.D., Shingai, R., Lunt, G.G., Goosey, M.W., Darlison, M.G., Sattelle, D.B., and Barnard, E.A. (1990). Sequence and functional expression of a single alpha subunit of an insect nicotinic acetylcholine receptor. EMBO J. *9*, 4391–4398.

Nasse, M.J., and Woehl, J.C. (2010). Realistic modeling of the illumination point spread function in confocal scanning optical microscopy. J. Opt. Soc. Am. -Opt. Image Sci. Vis. *27*, 295–302.

O'Haver, T. (2016). Intro. to Signal Processing:Deconvolution.

O'Shea, M., and Williams, J.L.D. (1974). The anatomy and output connection of a locust visual interneurone; the lobular giant movement detector (LGMD) neurone. J. Comp. Physiol. *91*, 257–266.

Osorio, D. (1986). Directionally selective cells in the locust medulla. J. Comp. Physiol. [A] *159*, 841–847.

Rind, F.C. (1984). A chemical synapse between two motion detecting neurones in the locust brain. J. Exp. Biol. *110*, 143–167.

Rind, F.C. (1987). Non-directional, movement sensitive neurones of the locust optic lobe. J. Comp. Physiol. A *161*, 477–494.

Rind, F.C. (2002). Motion detectors in the locust visual system: From biology to robot sensors. Microsc. Res. Tech. *56*, 256–269.

Rind, F.C., and Bramwell, D.I. (1996). Neural network based on the input organization of an identified neuron signaling impending collision. J. Neurophysiol. *75*, 967–985.

Rind, F.C., and Leitinger, G. (2000). Immunocytochemical evidence that collision sensing neurons in the locust visual system contain acetylcholine. J. Comp. Neurol. *423*, 389–401.

Rind, F.C., and Simmons, P.J. (1997). Signaling of object approach by the DCMD neuron of the locust. J. Neurophysiol. *77*, 1029–1033.

Rind, F.C., and Simmons, P.J. (1998). Local circuit for the computation of object approach by an identified visual neuron in the locust. J. Comp. Neurol. *395*, 405–415.

Rind, F.C., and Simmons, P.J. (1999). Seeing what is coming: building collision-sensitive neurones. Trends Neurosci. *22*, 215–220.

Rind, F., and Simmons, P. (1992). Orthopteran Dcmd Neuron - a Reevaluation of Responses to Moving-Objects .1. Selective Responses to Approaching Objects. J. Neurophysiol. *68*, 1654–1666.

Rowell, C.H.F. (1971). The orthopteran descending movement detector (DMD) neurones: a characterisation and review. Z. Für Vgl. Physiol. *73*, 167–194.

Rowell, C.H.F., O'Shea, M., and Williams, J.L.D. (1977). Rowell, C. H. F., O'Shea, M. & Williams, J. L. D. The neuronal basis of a sensory analyser, the acridid movement detector system. IV. The preference for small field stimuli. J. Exp. Biol. 68, 157-185. J. Exp. Biol. *68*, 157–185.

Stafford, R., Santer, R.D., and Rind, F.C. (2007). The role of behavioural ecology in the design of bio-inspired technology. Anim. Behav. *74*, 1813–1819.

Sztarker, J., and Rind, F.C. (2014). A look into the cockpit of the developing locust: Looming detectors and predator avoidance: Development of LGMDs and Hiding Behavior. Dev. Neurobiol. *74*, 1078–1095.

Takemura, S., Bharioke, A., Lu, Z., Nern, A., Vitaladevuni, S., Rivlin, P.K., Katz, W.T., Olbris, D.J., Plaza, S.M., Winston, P., et al. (2013). A visual motion detection circuit suggested by Drosophila connectomics. Nature *500*, 175–181.

Thany, S.H., and Tricoire-Leignel, H. (2011). Emerging pharmacological properties of cholinergic synaptic transmission: comparison between mammalian and insect synaptic and extrasynaptic nicotinic receptors. Curr. Neuropharmacol. *9*, 706.

Thany, S.H., Lenaers, G., Raymond-Delpech, V., Sattelle, D.B., and Lapied, B. (2007). Exploring the pharmacological properties of insect nicotinic acetylcholine receptors. Trends Pharmacol. Sci. *28*, 14–22.

Torkkeli, P.H., Widmer, A., and Meisner, S. (2005). Expression of muscarinic acetylcholine receptors and choline acetyltransferase enzyme in cultured antennal sensory neurons and non-neural cells of the developing mothManduca sexta. J. Neurobiol. *62*, 316–329.

Trimmer, B.A. (1995). Current excitement from insect muscarinic receptors. Trends Neurosci. *18*, 104–111.

Vizi, E.S., and Lendvai, B. (1999). Modulatory role of presynaptic nicotinic receptors in synaptic and non-synaptic chemical communication in the central nervous system. Brain Res. Rev. *30*, 219–235.

Wernitznig, S., Rind, F.C., Pölt, P., Zankel, A., Pritz, E., Kolb, D., Bock, E., and Leitinger, G. (2015). Synaptic connections of first-stage visual neurons in the locust Schistocerca gregaria extend evolution of tetrad synapses back 200 million years. J. Comp. Neurol. *523*, 298–312.

Wilson, D.M., Garrard, P., and McGinness, S. (1978). The unit structure of the locust compound eye. Cell Tissue Res. *195*, 205–226.

Wonnacott, S. (1997). Presynaptic nicotinic ACh receptors. Trends Neurosci. *20*, 92–98.

Young, H.S., Herbette, L.G., and Skita, V. (2003). alpha-bungarotoxin binding to acetylcholine receptor membranes studied by low angle X-ray diffraction. Biophys. J. *85*, 943–953.

# Appendix

## Animals

*Schistocerca Gregaria* were bought from ZOO Muser (Wiener Straße 186a, 8051 Graz).

## Equipment

| | |
|---|---|
| EMTRIM | Leica |
| FEI Tecnai G2 20 TEM | FEI |
| Laser Scanning Microscope TCS SP2 | Leica |
| Leica EM AC 20 | Leica |
| Light Microscope BX45 | Olympus |
| RTC basic hot plate with magnetic stirrer | IKA laboratory |
| Scale | Kern GS |
| Seven multi Mettler pH meter | Toledo |
| Ultramicrotome UCT | Leica |
| Ultrascan 1000 CCD Camera | Gatan |

## Chemicals and reagents

| | |
|---|---|
| Acetone | Merck |
| Bovine Serum Albumin | Sigma Aldrich |
| Chloroform | Merck |
| Ethanol absolute | Merck |
| Glutaraldehyde, 25% in H2O | Fluka BioChemika |
| Goat Serum | Sigma Aldrich |
| Na2HPO4*(H2O)2 | Merck |
| NaCl | Carl Roth |
| NaH2PO4*H2O | Merck |
| Nanoprobes HQ Silver Kit | Biotrend |
| Osmiumtetroxide (OsO4) | Electron Microscopy Service |
| Paraformaldehyde | Fluka BioChemika |
| Pro Long Gold Antifade Mountant | Life Technologies |
| PS-Speck™ Microscope Point Source Kit | ThermoFisher Scientific |
| stabilised Leadcitrate | Laurylab |
| Toluidine Blue | Agar Scientific LTD |
| Uranyl acetate 0.5% | Laurylab |

## Antibodies

| | |
|---|---|
| Cy2-conj. Goat-anti-mouse IgG | Dianova |
| Cy3-conj. Goat-anti-mouse IgG | Dianova |
| Nc82 | Gift from Prof. Erich Buchner (Würzburg), ANTIBODY_2314866 |
| Streptavidin-Nanogold conjugate | Biotrend |
| α-Bungarotoxin Alexa Fluor 488 | Life Technologies |
| α-Bungarotoxin Biotin conjugate | Life Technologies |
| α-Bungarotoxin-ATTO-633 | Alamone Labs |

## Immunohistochemistry buffer solutions

### Phosphate Buffered Saline (PBS)

| | |
|---|---|
| $Na_2HPO_4*12{\cdot}H_2O$ | 3,6g |
| $KH_2PO_4$ | 4,1g |
| NaCl | 8g |

Dissolve in about 800mL ddH2O, adjust the pH to 7.4 and fill up to 1000mL

### Phosphate Buffer (PB)

| | |
|---|---|
| $Na_2HPO_4*12{\cdot}H_2O$ | 14,47g |
| $NaH_2PO_4*H_2O$ | 1.325g |

Dissolve in about 800mL ddH20, adjust the pH to 7.4 and fill up to 1000mL

## Dissection Protocol

1. Pin the head with needles. Optional: cut away the antennae.

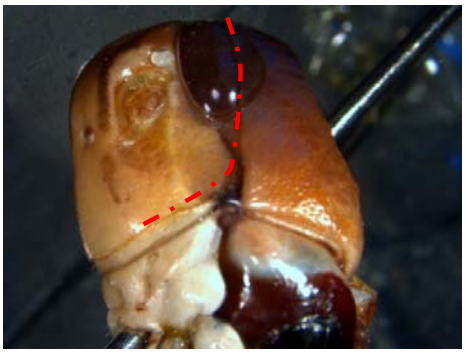

2. Cut from the eye to the back of the head capsule. Repeat on the other side.

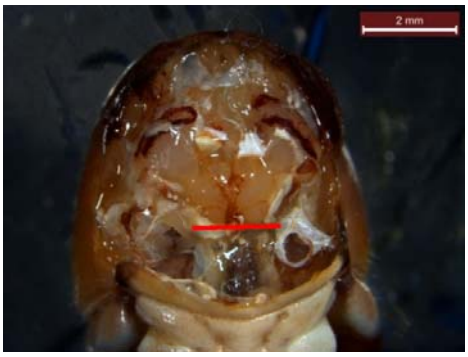


3. Pull the lid of the head off with tweezers, use tweezers to cut away fat tissue by pulling at a low angle just above the lobus opticus
4. Make a cut with small scissor at the designated connection, thus freeing the brain/lobus opticus part.

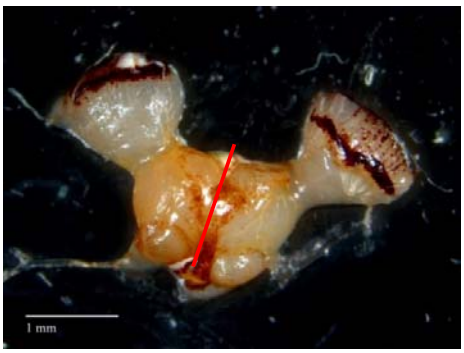


5. Take the lobus opticus with the brain part out and cut it in two parts at the designated line. Cut away residual fat.

*Pictures by Stefan Wernitznig, used here with permission*

## Visualization of NAChRs with Electron Microscopy

1. Immobilize animal on ice, dissect under ice-cold insect saline and immerse in ice-cold fixative.
2. Fix specimen for 3 hours in 2% paraformaldehyde diluted in 0.1M phosphate buffer (pH 7.4).
3. Rinse in phosphate buffer for 1 hour. /RT
4. Embed in gelatin (15% in PB) and fix for 2 hours (same fixative as above). /4°C
5. 0.1M phosphate buffer overnight
6. Cut 70µm sections with a vibratome.
7. Prepare **PBG**: 0.1M glycine, 0.8% BSA, 0.05% saponin in 0.013 M phosphate-buffered saline solution (**PBS**).
8. Preincubate 1: 0.05M glycine in PBS for 10 minutes to reduce electrostatic charge /RT
9. Preincubate 2: 5% normal goat serum in **PBG** 30 minutes. /RT
10. Incubate in 10nM bungarotoxin overnight (**diluted PBG**) /4°C
11. Rinse in PBG 3x15min. /RT
12. Incubate in streptavidin-nanogold 1:100 for 4 hours. /RT
13. Rinse in PBG 3x10min.
14. Postfix with 2%PFA/**2.5% GA** in 0.1M phosphate buffer for 30 minutes.
15. Rinse in PBG 3x10min.
16. Wash 3 times with 20mM citrate buffer for 5 minutes.
17. For HQ silver, use 3 drops of every solution per well (mix in between addition of every solution). 3 minutes reaction time in darkroom.
18. Rinse in 150 mM NaNO3 solution for 2x5min. Darkroom!
19. Immerse in 0.05% tetrachloroauric [III] acid in 150 mM Acetate buffer, ph 5.6, 7minutes. Darkroom!
20. Rinse in 150 mM NaNO3 solution for 2x5min.
21. Wash 2x10 minutes phosphate buffer.
22. 0.1M phosphate buffer overnight
23. Postfix 30 minutes in 1% osmium tetroxide solution.
24. Rinse 2x30 minutes in 0.1M phosphate buffer.

25. Dehydrate section in series of ethanol:
26. 50% ethanol – 20min
27. 70% ethanol – 20min
28. 80% ethanol – 20min
29. 96% ethanol – 20min
30. 100% ethanol – 2x10min
31. Propylenoxide – 30min
32. Propylenoxide/TAAB 1+1 – 3hours
33. Propylenoxide/TAAB 1+2 – overnight
34. TAAB – 2x1.5hours
35. Embedd in TAAB epoxy resin and cure for 3 days at 60°C.
36. Counterstain in lead citrate and platin blue.

## Visualization of NAChRs with Fluorescence Microscopy

1. Immobilize animal on ice, dissect under ice-cold insect saline and immerse in ice-cold fixative.
2. Fix brains 3 hours at room temperature in 2% paraformaldehyde (dissolved in 0.1 M phosphate buffer, pH 7.4).
3. Embed in gelatin (15% in PB) and fix for 2 hours (same fixative as above). /4°C
4. Rinse in phosphate buffer for 1 hour. /RT
5. Cut 50-70µm vibratome sections.
6. Transfer to 0.013 M phosphate-buffered saline solution (PBS), pH 7.4
7. Prepare **solution1** of 0.1% Triton X-100, 0.8% bovine serum albumin and 0.1M glycine in PBS, pH 7.4.
8. Preincubate the sections for 1 hour in 5% normal Goat serum in in **solution1** at room temperature.
9. Incubate overnight with primary antibody in **solution1**.
10. Rinse in PBS (3x10min).
11. Secondary antibody: fluorescent dye coupled goat anti-mouse (1:100-1:300) for 2 hours at room temperature in **solution1**.
12. Rinse in PBS (3x10min).
13. Transfer to destilled water.
14. Mount using ProLong Gold Antifade and surround coverslips with nail polish.